RSC Advances

PAPER

View Article Online
View Journal | View Issue

Cite this: *RSC Adv.*, 2024, **14**, 31502

Group 7 carbonyl complexes of a PNN-heteroscorpionate ligand†

Jorge P. Valdivieso, III, Alexander N. Erickson and James R. Gardinier *

A series of rhenium and manganese carbonyl complexes of a heteroscorpionate ligand with an atypical N_2P-donor set has been prepared to better understand their electronic and CO releasing properties. Thus, the ligand, pz_2TTP, with an *a,a*-bis(pyrazol-1-yl)tolyl group decorated with an *ortho*-situated di(*p*-tolyl)phosphanyl reacts with carbonyl group 17 reagents to give [*fac*-(κ^2NP-pz_2TTP)Re(CO)$_3$Br], **1**, and [*fac*-(κ^3N_2P-pz_2TTP)M(CO)$_3$](OTf = O_3SCF_3), **2-M** (M = Re, Mn), if care is taken during the preparation of the manganeses derivative. When heated in CH_3CN, **2-Mn** slowly transforms to [*fac*,*cis*-(κ^3N_2P-pz_2TTP)Mn(CO)$_2$(NCCH$_3$)](OTf), **3-Mn**. In contrast, the corresponding **3-Re** can only be prepared from **2-Re** using Me_3NO; pure **3-Mn** can also be prepared by this method. Experimental and density functional calculations at the M06L/Def2-TZVP/PCM(CH_3CN) level show that the replacement of a carbonyl with an acetonitrile solvent decreases the oxidation potential by around 0.8 V per carbonyl released, making decarbonylated species potent reductants. At the same time, the electronic spectrum broadens and undergoes a red-shift, making dicarbonyl complexes more susceptible to photo-initiated decarbonylation reactions than tricarbonyls. When **2-Mn** or **3-Mn** are irradiated in with 390 nm LED light in aerated solutions, [*trans*-Mn(pz_2TTP = O)$_2$](OTf)$_2$, **4**, along with insoluble manganese oxides are rapidly formed.

Received 21st July 2024
Accepted 24th September 2024

DOI: 10.1039/d4ra05287k

rsc.li/rsc-advances

Introduction

Group 7 carbonyl complexes have found diverse uses in catalysis[1–6] and medicinal chemistry.[7–14] Their utility is typically predicated on the stabilities of either $LM(CO)_3^+$ or $LM(CO)_2^+$ cores. Thus, the stability of $[Tc(CO)_3]^+$ complexes have been exploited in radiopharmaceutical imaging applications (^{99m}Tc, γ emitter, $t_{1/2}$ = 6.05 h). In contrast, manganese(I) tricarbonyl complexes are visible-light absorbing chromophores that readily lose all carbonyls on photo-excitation, making them useful as photoinduced CO releasing molecules (Photo-CORMs).[10,12,13,15,16] Five-coordinate $LMn(CO)_2$ pincer complexes are potent catalysts for a variety of chemical transformations.[2,17] Certain $Re(CO)_3^+$ complexes can lose one CO with either UV-irradiation (or more commonly by reaction with Me_3NO) to give highly reactive $Re(CO)_2^+$ species that can facilitate C–H bond activations.[18–20] Most recently, rhenium(I) carbonyl complexes have been investigated for their potent anti-cancer properties whose mode of action remains under investigation, but whose activity may be tied to the ability of the $Re(CO)_x^+$ (x = 2, 3) to interact with reactive oxygen species after binding to cellular matter.[7,8,21,22] Thus, in any new group 7 carbonyl complex, it is desirable to understand their CO releasing capabilities.

Facially coordinating tridentate ligands with two pyrazolyl and one non-pyrazolyl Lewis donor are heteroscorpionates[23–26] that are related to the more ubiquitous tris(pyrazolyl)methane (Tpm) and tris(pyrazolyl)borate (Tp), C-[27] and B-[24] scorpionate ligands, respectively.[28] For many catalytic and biomedical applications, heteroscorpionates are enticing since the unique donor can be suitably functionalized to elicit a desired reactivity. A variety of group 7 carbonyl complexes of heteroscorpionates with N_2N,[29–31] N_2O,[32–39] and N_2S[40,41] donor sets have been reported. Of these, the CO releasing properties of N_2N[29] and N_2O[35,42,43] complexes of $Mn(CO)_3^+$ have been studied in detail. It was found that under 365 nm irradiation the N_2O complexes with anionic bis(pyrazolyl)acetate, bpza, or bis(pyrazolyl)propionate, bpzp, ligands were more reactive ($t_{1/2}$ ~ 8 min^{-1}) than $[(Tpm)Mn(CO)_3]^+$ ($t_{1/2}$ ~ 11 min^{-1}) while the bulkier N_2N heteroscorpionates based on (*N*-4-*R*-benzyl)-bis(pyrazolyl)ethanamines, bpea^{BzR}, were less reactive ($t_{1/2}$ ~ 25 min^{-1}) under similar conditions. Moreover, the ultimate manganese products after photoinduced CO dissociation depended on the ligand, with $[Mn^{II}(Tpm)_2]^{2+}$ or [(κ^3-bpza)Mn^{II}(μ-κ^2N,κ^1O-bpza)]$_2$ and manganese oxides being isolated in the former cases. In bpea^{BzR} cases, carbonyl-free species were not identified, but the dicarbonyl and, for the first-time, a mono-carbonyl scorpionate species could be detected.[29] To

Department of Chemistry, Marquette University, Milwaukee, Wisconsin 53201-1881, USA. E-mail: james.gardinier@marquette.edu

† Electronic supplementary information (ESI) available: Spectra, computational details, xyz files of calculated structures, cif files, checkcif reports. CCDC 2371547, 2371549–2371553 and 2383876. For ESI and crystallographic data in CIF or other electronic format see DOI: https://doi.org/10.1039/d4ra05287k

our knowledge, the CO releasing properties of softer heteroscorpionates have not yet been reported. In 2014 our group reported on a new heteroscorpionate, pz_2TTP (Fig. 1, left),[44] with a rare N_2P donor set, joining $[Fc(PPh_2)(Bp^*)]^-$ (Fig. 1, right)[45,46] as the only other known example with such a donor set. In neither case has the group 7 chemistry been described.

The incorporation of a phosphorus donor into a heteroscorpionate was envisioned to be advantageous since the bulky and *trans*-labilizing diarylphosphine group might stabilize unusual low-oxidation state group 7 complexes such as di- or possibly even mono-carbonyls. Additionally, all complexes might be easily characterized by ^{31}P NMR spectroscopy. The findings of our initial investigation into the preparation, electronic properties, and potential CO-releasing reactivity of rhenium(I) and manganese(I) carbonyl complexes of pz_2TTP are detailed herein.

Results and discussion

Syntheses

Heating solutions containing pz_2TTP and an equimolar quantity of group 7 carbonyl reagents generally produced mixtures of compounds rather than high yields of a single compound. Scheme 1 provides a summary of optimized syntheses of the group 7 carbonyl complexes of pz_2TTP. Thus, the reaction between equimolar pz_2TTP and $Re(CO)_5Br$ in toluene gives the expected $(pz_2TTP)Re(CO)_3Br$, **1**, in modest yield after crystallization (Scheme 1, left). However, IR, NMR, single crystal and powder X-ray diffraction reveal this analytically pure sample to be a mixture of isomers (*vide infra*, Fig. S2–S4†). When an equimolar mixture of pz_2TTP, $Re(CO)_5Br$, and $Tl(O_3SCF_3 = OTf)$ are heated in CH_3CN, crystals of analytically pure $[(pz_2TTP)Re(CO)_3](OTf)$, **2-Re**, can obtained in modest yield; the crude material before crystallization shows evidence for the formation of minor (but variable) amounts of the dicarbonyl $[(pz_2TTP)Re(CO)_2(NCCH_3)](OTf)$, **3-Re**. A similar reaction with $Mn(CO)_5Br$ *in lieu* of the rhenium reactant affords mixtures of tricarbonyl **2-Mn** and dicarbonyl **3-Mn**, favouring the latter after heating 30 min (Fig. S10†). Instead, pure **2-Mn** is best prepared at low temperature by the reaction between pz_2TTP and $[fac\text{-}Mn(CO)_3(NCCH_3)_3](OTf)$. The pure dicarbonyls **3-M** (M = Re, Mn) are best prepared by decarbonylation of **2-M** by using equimolar anhydrous Me_3NO in CH_3CN. Although the reactions appear insensitive to an excess of Me_3NO, the separation from this reagent is tedious, so it is easiest to use one equivalent rather than an excess.

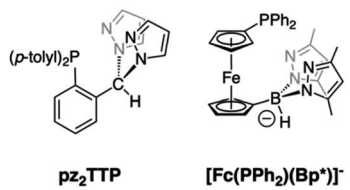

Fig. 1 Heteroscorpionate ligands with PNN donor sets.

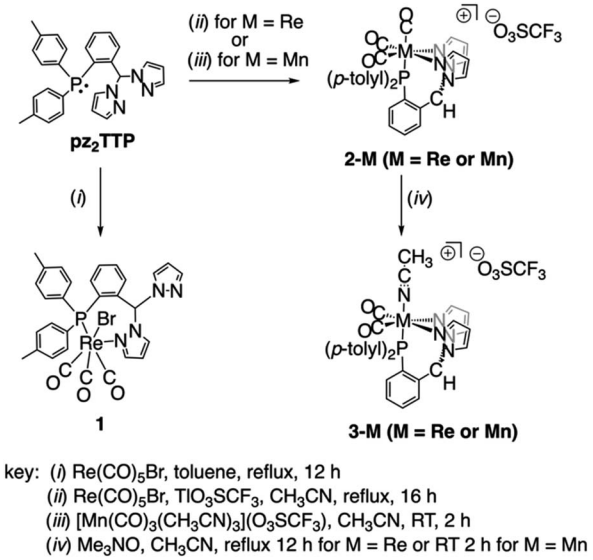

Scheme 1 Preparative routes to the various group 7 carbonyl complexes of pz_2TTP.

Solid state structures

The solid-state structures of representative rhenium carbonyl complexes of pz_2TTP are given in Fig. 2, those of the manganese derivatives are provided in Fig. S1 of the ESI.† Bond distances and angles for each compound are listed in Table 1. It is rare[47] for scorpionate complexes of $Re(CO)_3$ to exhibit a κ^2-binding mode instead of prototypical κ^3-mode. However, the crystals of **1** possess a κ^2NP-ligand bound to a *fac*-$Re(CO)_3Br$ moiety; one pyrazolyl ring remains "free". The resulting seven-membered (Re1–N12–N11–C7–C2–C1–P1) chelate ring folds into a boat conformation with the methine carbon C7 as the bow and the Re1–P1 bond as the stern of the boat. This conformation places the methine hydrogen H7 inside the boat and the "free" pyrazolyl outside (left two structures of Fig. 2). In **1**, there is a disorder that places either the bromide (Br1A; 80%) or a carbonyl (C10B–O3B; 20%) inside the boat. The disorder leads to greater uncertainty Re–C9A/B distances than other Re–C distances. For the well-behaved carbonyls, the Re1–C10 bond *trans*- to P1 (1.977(4) Å in **1**) is significantly longer than that *trans*- to the pyrazolyl nitrogen (Re1–C8: 1.924(4) Å). The Re1–C8 distance compares favourably with the average Re–C distance of 1.92(1) Å in either $[fac\text{-}(\kappa^3\text{-}HCpz_3)Re(CO)_3]Br$[48] or $[fac\text{-}(\kappa^3\text{-}CH_3CH_2Cpz_3)Re(CO)_3](O_3SCF_3)\cdot 1.5H_2O\cdot 0.5CH_3CN$,[49] or of 1.91 Å in $[fac\text{-}(\kappa^3\text{-}HCpz^{3iPr}{}_3)Re(CO)_3]Br\cdot$acetone.[50] Thus, the longer Re–C distance in **1** is a manifestation of the significantly greater *trans*-influence of the ditolylphosphanyl *versus* a pyrazolyl moiety. It is noted that the Re–N bond distance of 2.209(3) Å in **1** is a little longer than found in other rhenium scorpionates that typically range from 2.14 to 2.19 Å: $Re–N_{avg}$ 2.18 Å for $[fac\text{-}(\kappa^3\text{-}HCpz_3)Re(CO)_3]Br$[48] 2.16 Å for $[fac\text{-}(\kappa^3\text{-}CH_3CH_2Cpz_3)Re(CO)_3]^+$ (ref. 49) or 2.14 Å for $\{1,4\text{-}C_6H_4[CH_2OCH_2Cpz_3Re(CO)_3]_2\}^{2+}$ for instance.[50] The longer Re–N bonds in **1** are due to the charge neutral-nature of the $Re(CO)_3Br$ core and to the significantly greater steric profile of the *p*-tolyl$_2$P group relative to a pyrazolyl.

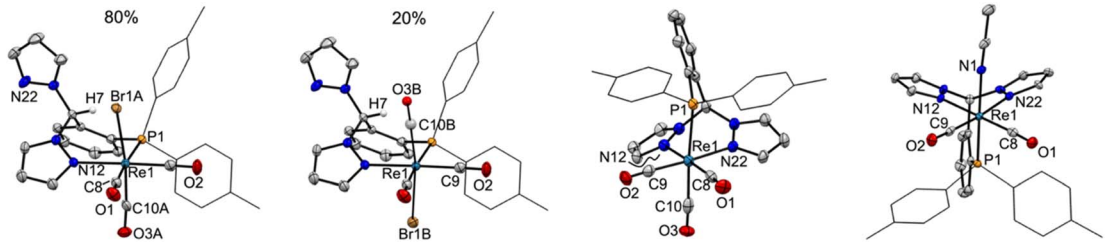

Fig. 2 (Left): Views of major and minor disorder components in **1**, highlighting isomers; (Centre): view of the cation in **2-Re**; (Right): view of the cation in **3-Re**. Ellipsoids are drawn at the 50% probability level.

Such long Re–N bonds are also evident in [*fac*-(κ^3-N_2O bpza)$Re(CO)_3$] (Re–N_{avg} 2.21 Å)[34] and in the complex of a pyridyl based P-scorpionate [*fac*-(κ^2N–P(py)$_3$)$ReBr(CO)_3$] (Re–N_{avg} 2.21 Å).[47]

The replacement of the bromide in **1** with a triflate results in a shift in ligand binding mode to give [*fac*-($\kappa^3$$N_2$P-$pz_2$TTP)$Re(CO)_3$](OTf), **2-Re** (third structure, Fig. 2) with an unbound anion. The lower electron density at the metal centre in the cation relative to **1** results in shorter metal-scorpionate bonds and, due to lower capacity for pi back-bonding, longer Re–C bonds than in **1**. Thus, the Re1–P1 bond in **2-Re** of 2.47 Å is 0.02 Å shorter than that in either **1** or its CH_2Cl_2 solvate. The average Re–N bonds in **2-Re** of 2.18 Å are 0.03 Å shorter than in **1** and are comparable to those in [*fac*-(κ^3-$HCpz_3$)$Re(CO)_3$]Br.[48] Moreover, the average Re–C bond in **2-Re** of 1.95 Å is about 0.01 Å longer than that in **1**. As with **1**, the Re1–C10 bond in **2-Re** 1.978(5) Å is significantly longer than those bonds *trans*- to pyrazolyl nitrogens (Re1–N12 1.924(5) Å, Re1–N22 1.936(5) Å).

The related complex [*fac*-($\kappa^3$$N_2$P-$pz_2$TTP)$Mn(CO)_3$](OTf), **2-Mn**, despite having a formula similar to **2-Re**, crystallizes in the monoclinic space group $P2_1/c$, rather than $P\bar{1}$, like its heavier congener. Many of the structural features observed in **2-Re** are preserved in **2-Mn**, but the smaller size of Mn relative to Re gives shorter bonds. Thus the average Mn–N bond distance of 2.05 Å is 0.13 Å shorter than in **2-Re** but is similar to that found in other C-scorpionate complexes of $[Mn(CO)_3]^+$ such as 2.03 Å in [$(HCpz_3)Mn(CO)_3$](PF_6),[51] 2.05 Å in [$(Hpz(3\text{-}CHpz_2))Mn(CO)_3$]($O_3SCF_3$),[31] or 2.07 Å found in [$HC(3\text{-}iPrpz)_3Mn$-$(CO)_3$](O_3SCF_3).[52] The average Mn–C distance of 1.82 Å in **2-Mn** is 0.13 Å shorter than that in **2-Re** and is comparable to 1.81 Å found for all three of the aforementioned manganese C-scorpionates. Again, in **2-Mn**, the Mn1–C10 bond *trans*- to the P atom is significantly longer than the other two Mn–C bonds (1.841(2) Å *vs.* 1.806(2) and 1.814(2) Å).

Finally, the replacement of the CO *trans*- to phosphorous in **2-Re**, with an acetonitrile gives [*fac*,*cis*-(pz_2TTP)

Table 1 Selected Bond distances (Å) and interatomic angles (°) in group 7 carbonyl complexes of pz_2TTP

Compound	**1**	**2-Re**	**2-Mn**	**3-Re**	**3-Mn** [a]
Bond					
M–Br1	2.6057(11)				
M–P1	2.4892(10)	2.4734(10)	2.3350(5)	2.3510(10)	2.2784(3)
M–N1				2.118(4)	2.0107(15)
M–N12	2.209(3)	2.185(3)	2.0580(14)	2.180(3)	2.0550(11)
M–N22		2.183(4)	2.0437(14)	2.158(4)	2.0359(11)
M–C8	1.925(4)	1.924(5)	1.8062(17)	1.914(5)	1.8005(14)
M–C9	1.907(9)	1.936(5)	1.8139(18)	1.890(5)	1.7806(14)
M–C10	1.976(4)	1.978(5)	1.8409(18)		
Angles					
N12–M–N22		84.38(13)	88.32(5)	84.82(13)	88.08(4)
P1–M–N12	94.78(9)	91.27(10)	89.09(4)	89.53(9)	88.74(3)
P1–M–N22		80.72(9)	84.90(4)	90.01(9)	89.99(3)
C8–M–C9	91.9(3)	86.73(19)	87.71(7)	88.79(18)	86.80(6)
C8–M–C10	88.50(17)	89.35(18)	86.96(7)		
C9–M–C10	90.2(3)	87.97(18)	91.27(7)		
Br1–M–N12	85.60(9)				
Br1–M–P1	93.22(3)				
N1–M–P1				169.78(10)	171.16(8)
C10–M–P1	175.18(12)	175.23(13)	175.48(5)		
N12–M–C8	178.37(15)	176.94(16)	178.56(6)	179.53(16)	176.84(5)
N22–M–C9		177.11(16)	177.53(7)	174.89(15)	176.27(5)

[a] Only values for major disorder component of **3-Mn$_{0.92}$2-Mn$_{0.08}$** are given.

$M(CO)_2(NCCH_3)][OTf)$, **3-Re**. Interestingly, while the corresponding analytically and spectroscopically pure **3-Mn** can be prepared, it has not been possible to obtain single crystals suitable for X-ray diffraction. Instead, suitable X-ray quality single crystals of **3-Mn** co-crystallized with small portions of **2-Mn** (see experimental) can be obtained. The following structural discussion refers to the metrics found in the major disorder component in **3-Mn$_{0.92}$2-Mn$_{0.08}$**. The lower *trans*-influence of CH_3CN relative to CO affords a shorter M1–P1 bond in **3-M** (2.3510(10) Å for M = Re, 2.2784(3) Å for M = Mn) *versus* that in **2-M** (2.4734(10) Å for M = Re and 2.3350(5) Å for M = Mn). A secondary effect of the replacement of CO for CH_3CN is a slight shortening of M–C bonds (Re–C_{avg} = 1.902 Å and Mn–C_{avg} = 1.795 Å) *versus* those in **2-M** due to an increased electron density at the metal centre that strengthens the pi-back-bonding to the remaining CO groups, as will be detailed more fully below. Surprisingly, while there are multiple structurally characterized dicarbonylrhenium(I) B-scorpionate complexes,[53,54] to the best of our knowledge, **3-Re** is the first structurally characterized dicarbonylrhenium(I) C-scorpionate complex. C-scorpionates of $[Re(CO)_2(NO)]^+$ are known[55] but are not structurally characterized. The average Re–C bond in **3-Re** is more aligned with that in $[(HBpz_3 = Tp)Re(CO)_2]_2(\mu\text{-}N_2)$ (1.91 Å)[54] than those found in either $TpRe(CO)_2(THF)$ (1.872 Å) or $TpRe(CO)_2(PPh_3)$ (1.88 Å).[53] The structure of **2-Mn** is also noteworthy since there are relatively few structurally characterized C-scorpionate complexes of the $[cis\text{-}Mn(CO)_2]^+$ moiety, with $[(HC(3,5\text{-}Me_2pz)_3 = Tpm^*)Mn(CO)_2(L)](PF_6)$ (L = PMe_3, py)[56] being examples. In both of these latter cases, with more electron-donating 3,5-dimethylpyrazolyls, the average Mn–C bond of 1.76 Å is slightly shorter than that in **3-Mn** (1.79 Å).

Spectroscopic studies

The identity of each species **1**, **2-M**, and **3-M** can be easily distinguished by ^{31}P and ^1H NMR spectroscopy, with the former being easiest to interpret since singlet resonances are observed in most cases (*vide infra*). That is, while the stable isotopes of group 7 metals used here all have nuclear spin $I = 5/2$, (abundance: ^{55}Mn (100%), ^{185}Re (37.4%), ^{187}Re (62.6%)), each isotope has a large nuclear quadrupole moment Q_o (^{55}Mn: +0.330(10), ^{185}Re: +2.18(2), ^{187}Re: +2.07(2) barn)[57] that causes rapid relaxation on the NMR timescale, so that a singlet rather than the expected (1 : 1 : 1 : 1 : 1 : 1) sextet resonance is observed in ^{31}P NMR spectrum of each compound. Thus, the ^{31}P NMR spectrum of analytically pure prism crystals of **1** in CD_3CN gives two singlets at δ_P 10.5 (80% rel. int.) and 0.3 (20% rel. int.) ppm for its two co-crystallized isomers (Fig. S3 and S4†). The ^1H NMR spectrum of **1** also shows two sets of resonances in a 4 : 1 ratio (Fig. S3†), that are most easily distinguished by the two unequal pairs of characteristic H_4-pyrazolyl resonances near δ_H ~6.1 and δ_H ~6.3 ppm, assigned to "free" and Re-bound pyrazolyls, respectively, of each isomer in accord with the solid-state structures. These assignments are made by comparison with the spectra of the free ligand (δ_H = 6.10 ppm) and other Re complexes (*vide infra*). The ^{31}P NMR spectrum of **2-Re** has a singlet resonance at δ_P 4.5 ppm while that of **3-Re** occurs more downfield at 17.9 ppm. Similarly, a singlet is observed for **2-Mn** at δ_P = 33.8 ppm and for **3-Mn** at δ_P 66.3 ppm.‡ The ^1H NMR spectrum of each **2-M** and **3-M** (Fig. S6–S9†) is aligned with expectations that solid state structures are maintained in CD_3CN solution with one set of resonances that are significantly shifted with respect to those of the free ligand. Particularly diagnostic are resonances for H_4-pyrazolyls. For the rhenium compounds, these occur at δ_H 6.58 for **2-Re** and δ_H 6.51 for **3-Re**, both shifted downfield with respect to that of the free ligand at δ_H 6.10 ppm. Here, the more electron rich **3-Re** is shifted upfield from **2-Re**, as expected. The analogous resonances for manganese derivatives are shifted further downfield (δ_H 6.63 for **2-Mn** and δ_H 6.57 for **3-Mn**) than in the rhenium cases, consistent with greater Lewis acidity of the 3rd *versus* 5th row metal. Other diagnostic resonances occur for tolyl and unique aromatic ring hydrogens. An unusual feature of the ^1H NMR spectra of each **2-M** and **3-M** is that the most downfield resonances for acidic methine H_α, the H_5-pyrazolyl ring, and the H_3-aryl (positioned *ortho*- to the $CHpz_2$ group) hydrogens exhibit concentration dependent shifts in the 10^{-3} to 10^{-4} M range. The magnitude of concentration-dependent chemical shift changes, $|\Delta\delta_H|$, falls in the order H_α > H_5pz > H_3Ar consistent with their decreasing relative acidities (Fig. S11†). It is noted that close contacts occur between the triflate ion and these hydrogens in the solid state structures of **2-M**. Presumably these concentration dependent shifts are the result of contact ion pairs forming that are favoured at high concentration with triflate oxygens causing the observed shifts to lower fields, as seen in other systems.[31,58–65] Finally, although resonances for most carbons could be observed, rapid quadrupolar relaxation in combination with the expected $^2J_{C-P}$ coupling (splitting signal intensity) inhibited observation of resonances for CO groups in the ^{13}C NMR spectrum of tricarbonyl complexes reported here.

The IR spectra of each complex was recorded in both the solid state and in CH_3CN solution. A summary of solution data is found in Table 2 while other data are provided in the ESI (Fig. S12 and S13).† In the group 7 tricarbonyl compounds **1** and **2-M** three bands were observed for CO stretches consistent with a *fac*-$M(CO)_3$ arrangement, as observed in the solid state. The low symmetry coordination environment imposed by the scorpionate about the metal in ensures that the A_1 and E bands of a nominally C_{3v} symmetric $M(CO)_3$ core are split into two A′ and

‡ As with many other systems (*e.g.*; see δ_P's of $XPCl_3$ X = O, S, Se), there are no simple explanations for the observed trends in ^{31}P NMR chemical shifts for the **2-M**, and **3-M** series. The shift δ_P depends on many competing factors like bond-distance (diamagnetic contribution) and on paramagnetic terms such as bond angles, relative electronegativities, as well as d- and p- π-bonding contributions.[94–97] In the current cases, there is a parabolic relation between the Mulliken charge on phosphorus and chemical shift (see Fig. S22 of the ESI†) that, in turn, may be the result of many of the above factors. The shorter bond distance and greater spectroscopic electronegativity of Mn (χ_{spec} (Mn) = 1.75 (Pauling units) *vs.* χ_{spec} (Re) = 1.59)[98,99] *versus* Re may be ultimately responsible for downfield shift in Mn *versus* Re complexes. It is noted that Pauling electronegativities are reverse order of spectroscopic electronegativities ($\chi_{Pauling}$ (Mn) = 1.55 *vs.* $\chi_{Pauling}$ (Re) = 1.90). For a given metal, the differences in chemical shifts between **2-M** and **3-M** counter expectations. The more electron rich **3-M** (with shorter M–P bonds due to increased M → P backbonding) is shifted downfield relative to **2-M**; the reverse trend might be expected.

Table 2 Summary of solution (CH_3CN) IR data for CO stretching modes, ν_{CO} (cm^{-1})

Compound				Avg.	Calcd[a]
1	2030	1936	1893	1953	1944
2-Re	2035	1938	1921	1965	1959
2-Mn	2038	1958	1933	1976	1981
3-Re		1944	1871	1908	1903
3-Mn		1959	1880	1921	1930

[a] Average values from M06L/def2-TZVP/PCM, CH_3CN (see ESI).

one A″ modes in C_s symmetry (**2-M**) or thee A modes in C_1 symmetry (complex **1**). The average energy for CO stretches decreases with increasing electron donating ability of the metal centres due to increased metal to ligand π-backbonding. Thus, the average CO stretch in charge neutral **1** ($\bar{\upsilon}_{CO\ avg} = 1953\ cm^{-1}$) is lower than in cationic **2-Re** ($\bar{\upsilon}_{CO\ avg} = 1965\ cm^{-1}$), albeit comparison may be somewhat inappropriate given the different supporting ligands (κ^2NP- *vs.* κ^3N_2P-). Next, consistent with expectations based on both orbital overlap and spectroscopic electronegativity, the CO bonds in **2-Re** are weaker than those in **2-Mn** ($\bar{\upsilon}_{CO\ avg} = 1976\ cm^{-1}$). Similar trends are found in $TpM(CO)_3$ ($\bar{\upsilon}_{CO\ avg} = 1951\ cm^{-1}$ for Re[20,53,66] and $1964\ cm^{-1}$ for Mn[20,67]), $[(Tpm)M(CO)_3]^+$ $\bar{\upsilon}_{CO\ avg} = 1973\ cm^{-1}$ for Re[50] and $1988\ cm^{-1}$ for Mn,[43,51,52] and in heteroscorpionate cases $[(bpza)M(CO)_3]$[34] ($\bar{\upsilon}_{CO\ avg} = 1952\ cm^{-1}$ for Re and $1971\ cm^{-1}$ for Mn). As noted for $TpM(CO)_3$ *versus* $[(Tpm)M(CO)_3]^+$, charge neutral Tpm derivatives give cationic complexes with higher energy CO stretches than their anionic B-scorpionate counterparts. The electron donating ability of pz_2TTP gives complexes with CO stretches intermediate between those of neutral and anionic NNN-based homoscorpionates. The IR spectra of the dicarbonyls, **3-M**, consist of two equal-intensity bands for symmetric and asymmetric CO stretches. Again, the heavier group 7 congener has lower energy stretches ($\bar{\upsilon}_{CO\ avg} = 1903\ cm^{-1}$) than the lighter congener ($\bar{\upsilon}_{CO\ avg} = 1930\ cm^{-1}$). The CO stretches in each dicarbonyl **3-M** are lower energy than in the tricarbonyl variants **2-M** since the replacement of a CO with a less π-acidic CH_3CN allows the metals to redistribute their electron density into the remaining CO antibonding orbitals.

Electronic properties

To facilitate discussion of the electronic properties of the new complexes, it will be useful to briefly examine the frontier orbitals of **2-M** and **3-M** as elucidated from DFT calculations performed at the M06L/def2-TZVP/PCM (CH_3CN) level of theory. As might be expected, the frontier orbitals of the four complexes share many similarities. A view of those orbitals in the cation of **2-Re** are given in Fig. 3, others are provided in the ESI, Fig. S18–S20.† The relative energy levels of related orbitals are provided in Fig. 4. First, all four complexes, **2-M** and **3-M**, possess mirror symmetry (C_s point group) where the mirror is assigned as the *yz*-plane that bisects the N12–M–N22 bond angle and contains the M–P bond. As such, the d_z2 and d_{xy} orbitals (both A′ representations) are directed along bonds. The d_x2-_y2 (A′ representation), d_{yz} and d_{xz} (both A″ representations) orbitals are located between bonds and are involved in pi-bonding interactions. For each complex, the three highest-energy filled orbitals, HOMO($-N$) ($N = 0, 1, 2$), are mainly metal-centred with

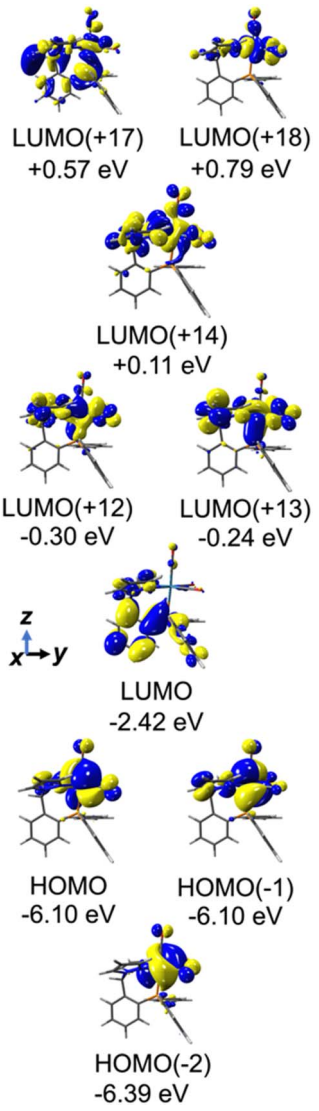

Fig. 3 Frontier orbitals of **2-Re**.

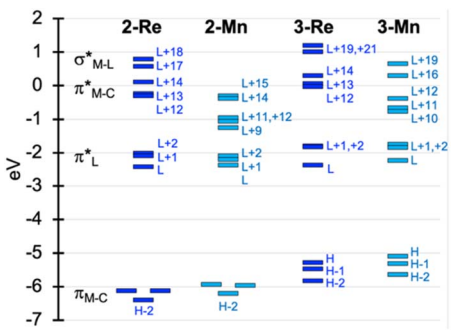

Fig. 4 Energy levels of frontier orbitals in **2-M** and **3-M** (M = Re, Mn).

pi-bonding interaction with the carbonyl carbon, see bottom three orbitals Fig. 3 and those labelled π_{M-C} in the left of Fig. 4. The π_{M-C} orbitals of rhenium complexes are lower energy than the corresponding manganese derivatives. Moreover, those in **2-M** are lower energy than those of **3-M**. The corresponding antibonding counterparts (labelled π^*_{M-C}, Fig. 4 left) are found above LUMO(+8) (LUMO+12 to +14 for **2-Re**). The LUMO(+*N*) (*N* = 0–8) are mainly ligand-centred π-orbitals. For **2-Re**, LUMO(+17) and LUMO(+18) exhibit σ*-antibonding interactions between the scorpionate donor atoms and metals' d_z2 and d_{xy} orbitals, respectively. Similar interactions are found at higher energy in LUMOs (+19 and +21) in **3-Re**. In manganese cases, analogous interactions are found in LUMO(+14) or above, as shown in Fig. 4 and S18.† However, there is extensive mixing of A′ orbitals, so that σ* interactions are also found in LUMOs (+1 and +2) and, for **3-Mn**, in LUMOs (+5 and +7).

The electronic absorption spectrum for each rhenium complex recorded in CH_3CN consists of ligand centred bands below 275 nm ($\varepsilon > 20\,000$ M^{-1} cm^{-1}, Fig. S14†) that, at their low energy edge, overlap weak metal ligand charge transfer (MLCT) bands as suggested by TD-DFT calculations at the M06L-TZVP/PCM(CH_3CN) level. Electron density difference plots for 2-Re (Fig. S21†) show depletion of charge density at the $ReCO_3$ fragment and accumulation of density at the ligand aryl (for HOMO(−*N*) to LUMO transitions, *N* = 0, 1, 2). For **2-Re**, the onset of the MLCT band is near 340 nm, and the remaining spectra is featureless in the visible region, consistent with its colourless nature. For **3-Re**, the MLCT band onset occurs near 375 nm, giving rise to its faint yellow colour in solution (and the solid). In contrast, **2-Mn** and **3-Mn** are yellow orange. Their absorption spectrum (Fig. 5) each feature ligand centred bands like those for the rhenium derivatives but also feature medium intensity (ε ~1000–4000 M^{-1} cm^{-1}) MLCT bands in the violet (**2-Mn**) to blue (**3-Mn**) region of the visible spectrum, assigned based on intensities of bands, comparisons with related compounds, and on TD-DFT calculations. That is, the lowest energy band in the spectrum of **2-Mn** occurs at 350 nm (ε = 2800 M^{-1} cm^{-1}) which is comparable to the similar band in [(Tpm)Mn(CO)$_3$](PF$_6$) (λ_{max} (EtOH) = 349 nm, ε = 2200 M^{-1} cm^{-1}) or in [(bpza)Mn(CO)$_3$] (λ_{max} (EtOH) = 361 nm, ε = 1800 M^{-1} cm^{-1}).[42] TD-DFT calculations on **2-Mn** show that the lowest energy band is comprised of MLCT transitions between filled orbitals HOMO(−*N*) (*N* = 0, 1) involving Mn(CO)$_x$ (*x* = 3, 2) chromophores and virtual orbitals on the scorpionate pi-system, LUMO and LUMO(+1). The red shift for similar transitions in **3-Mn** compared to **2-Mn** is a consequence of the higher energy of the HOMO(−*N*) (*N* = 0, 1) in the former *versus* the latter.

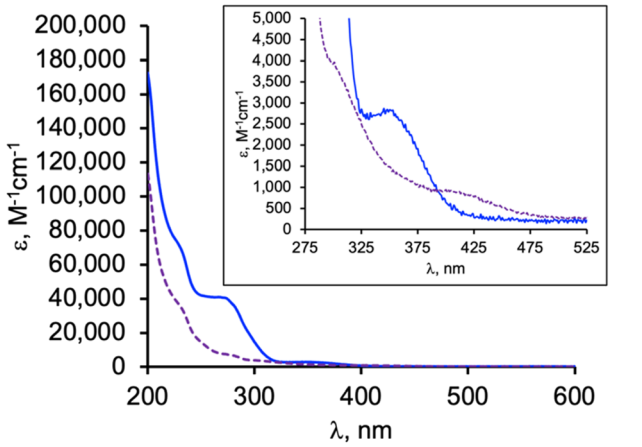

Fig. 5 Overlay of electronic absorption spectra of **2-Mn** (solid blue line) and **3-Mn** (dashed purple line) in CH_3CN. (Inset) Shows a close-up of the lowest energy bands.

The electrochemical properties of the complexes were examined by cyclic voltammetry in CH_3CN, as summarized in Table 3. Most voltammograms exhibit irreversible (i_{pc}/i_{pa} << 1) oxidation waves, apart from that of **3-Re** whose oxidation appears reversible (Fig. S15†). An irreversible reduction is observed for **2-Mn**, but no clear reduction events were observed within the solvent window for other complexes. Given the uncertainties in assigning potentials for electrochemically irreversible waves, the electrochemical processes were also estimated *via* theoretical calculations (M06L/Def2-TZVP/PCM(CH_3CN), Table 3, and ESI†). The computed values are 100 to 400 mV more negative than the observed values, but otherwise mirror observed trends. In each series **2-M** or **3-M** both the oxidation and reduction of the manganese derivatives are more favourable than for the corresponding rhenium analogues. Thus, oxidation of **2-Re** was found to be 320 mV (and calculated to be 300 mV) more positive than **2-Mn**. The reduction of **2-Re** was calculated to be only 80 mV more negative than **2-Mn**, consistent with the mainly ligand-centred LUMO. Moreover, for each metal, the replacement of a carbonyl group with an acetonitrile causes the oxidation to become more negative by about 600 mV experimentally (calculated to be 930 mV and 740 mV more negative for Mn for Re, respectively). Such behaviour mirrors that in other group 7 dicarbonyl scorpionates: [TpRe(CO)$_2$(THF)] $E_{1/2}$ = +0.42 V *vs.* NHE[54] *versus* [TpRe(CO)$_3$] $E_{1/2}$ = +1.41 V *vs.* NHE,[66] [(Tpm)Mn(CO)$_2$(CH$_3$CN)] $E_{1/2}$ = +0.58 V *vs.* NHE *versus* [(Tpm)Mn(CO)$_3$] $E_{1/2}$ = +1.53 V *vs.* NHE,[43] and [(bpza)Mn(CO)$_2$(CH$_3$CN)] $E_{1/2}$ = +0.29 V *vs.* NHE *versus* [(bpza)Mn(CO)$_3$] $E_{1/2}$ = +1.09 V *vs.* NHE[43]

Photo-induced CO release

As expected from the electronic spectra that are devoid of strong absorption bands in the visible region, colourless solutions of **1**, **2-Re**, or pale-yellow solutions of **3-Re**, are stable toward visible light. On the other hand, irradiation of a CH_3CN solution 20 mM in **2-Re** with a 38 W UV-C 254 nm light causes CO release with $t_{1/2}$ ~ 26 min to initially give **3-Re**, Fig. 6. This behaviour provides another rare example along with Tp*Re(CO)$_3$, of a rhenium-based CO releasing molecule. Interestingly, complex **3-Re** only undergoes slow and partial photodecomposition under these conditions. First, a new species with an asymmetric metal environment is formed, as indicated by two new sets of pyrazolyl resonances in the ^{1}H NMR see the two new H$_4$pz resonances in the top of Fig. 6 at δ_H 6.62 and 6.44 ppm. The ^{31}P NMR (Fig. S16†) also shows a new resonance at δ_p = 6.6 ppm.

Table 3 Summary of experimental (CH_3CN) and calculated (M06L/def2-TZVP/PCM(CH_3CN)) electronic properties of group 7 scorpionates

Compound	$E^{\circ}_{(MII/MI)}$ [a] (V)	$E^{\circ}_{(MI/M0)}$ (V)	λ [b] nm (ε, M^{-1} cm^{-1})
1	+1.72	—	268 (9000), 305 sh (3000), 341 sh (850)
$\mathbf{1}_{calc}$	+1.34	−2.05	279 (3600), 302 sh (2000), 346 (500)
2-Re	+1.95	—	243, (34 100), 268 (37 000)
2-Re$_{calc}$	+1.82	−1.92	275 (7500), 322 sh (500)
2-Mn	+1.63	−1.41	270 (40 800), 350 (2800)
2-Mn$_{calc}$	+1.52	−1.84	288 (4900), 326 (3150)
3-Re	+1.35	—	232 (78 400), 270 (30 300), 306 (13 500)
3-Re$_{calc}$	+1.08	−2.12	284 (6850), 322 (5200), 389 sh (325)
3-Mn	+0.99	—	274 (7500), 300 sh (3900), 405 (900)
3-Mn$_{calc}$	+0.59	−2.09	314 (4100), 357 (2600), 445 sh (260)

[a] V *versus* NHE; NBu_4PF_6 as supporting electrolyte. [b] Calculated TD-DFT spectra fit as sum of gaussian curves with $\sigma = 0.2$ eV.

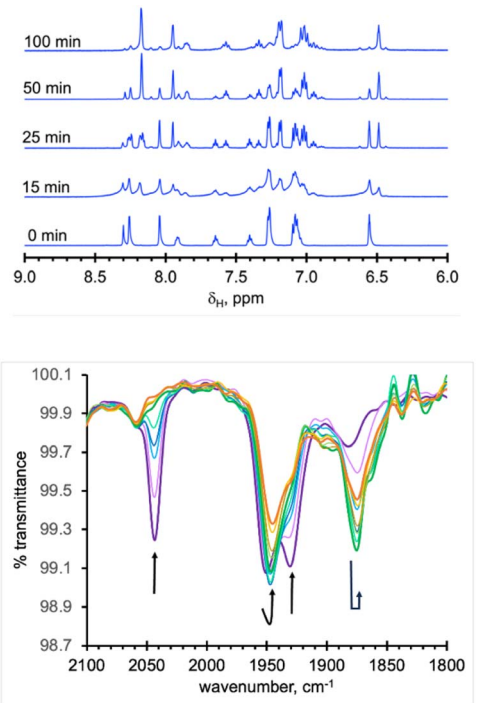

Fig. 6 (Top): Overlay of downfield region of ^{1}H NMR spectra of a CD_3CN solution initially 20 mM in **2-Re** (0 min), then at various stages after irradiation with 254 nm light; (Bottom): overlay of IR spectra of these solutions over similar time period (0 min, thicker purple line) but extended to 360 min (thicker orange line), showing conversion of **2-Re** first to **3-Re**, then the partial disappearance of the latter after 180 min (thicker green line).

The integrations indicate the new species reaches a maximum concentration of about 20% relative to **3-Re.** We tentatively assign this new species as either [*cis*-(κ^2PN-pz_2TTP)Re(CO)$_2$(κ^2O-OTf)] or [*cis*-(κ^2PN-pz_2TTP)Re(CO)$_2$(κ^1O-OTf)(CH_3CN)]. This assignment is based on the similarity of the ^{31}P NMR resonance and ^{1}H NMR resonances with **1**, as well as the shoulders on the low energy side of the two CO stretching bands of **3-Re.** It is less likely that the new species is a monocarbonyl, like [*cis*-(κ^3PN$_2$-pz_2TTP)Re(CH_3CN)$_2$(CO)](OTf), as there is no signal in the expected 1820–1830 cm^{-1} range. Upon continued irradiation (after 180 min) the NMR and IR signals for all species slowly disappear; the NMR spectra begin to show broad lines associated with paramagnetic species. We have not yet been able to identify the ultimate products of photodecomposition. In contrast, irradiation of 2 mM solutions of **2-Mn** in CH_3CN under normal atmosphere with a 50 W 390 nm LED light source (a source that matches well with the MLCT band) causes rapid and complete CO release in under 20 minutes with a first order decay half-life of $t_{1/2}$ = 3 min, indicated by UV-vis and IR

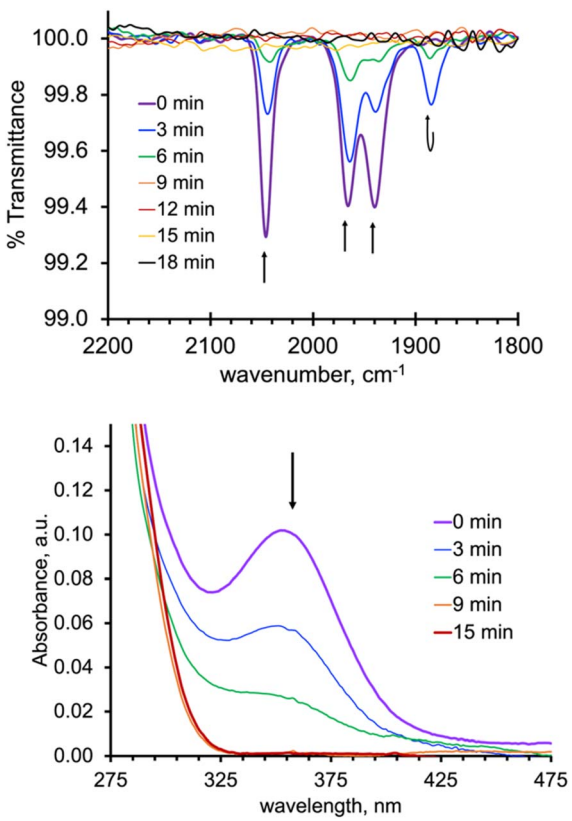

Fig. 7 (Top): Overlay of IR spectra of solutions initially 2 mM **2-Mn** recorded before and at 3 min intervals while irradiating with 390 nm light; (Bottom): UV-visible spectra of same solutions filtered to remove oxides and diluted to 10^{-5} M.

spectroscopy, Fig. 7. Here, **3-Mn** is an observable intermediate (1880 cm^{-1} IR band). During irradiation, the original yellow solution becomes a suspension of an insoluble brown precipitate (presumably amorphous manganese oxides) amidst a colourless solution (Fig. S17†). The colourless soluble component was identified as centrosymmetric *trans*-[Mn^{II}(κ^2NO-pz_2TTPO)$_2$(κ^1O-OTf)$_2$], **4**, by single crystal X-ray diffraction (Fig. 8). Aside from **3-Mn** when starting from **2-Mn**, no definitive intermediates have yet been identified which makes it difficult to pinpoint a favoured mechanistic sequence to give **4** at this time. Given the redox properties of **2-Mn** and **3-Mn**, a photoinduced release of CO's could also produce [(pz_2TTP)Mn(CO)(CH_3CN)$_2$]$^+$ or [(pz_2TTP)Mn(CH_3CN)$_3$]$^+$ that are predicted to have Mn^{2+}/Mn^+ ground state reduction potentials of +0.39 and −0.35 V *vs.* NHE, respectively. Neither is sufficiently negative to directly reduce O_2 to O_2^- in CH_3CN (−0.6 V *vs.* NHE)[68,69] but with a proton source (adventitious water) or if these act as Lewis acids capable of inner sphere e^- transfer, they might be capable or reduction (empirical limit +0.6 V *vs.* NHE).[70,71] If O_2 reduction occurs, the resulting manganese(II) species could symmetrize (ligand redistribution) to form [Mn(pz_2TTP)$_2$]$^{2+}$ and [Mn(CH_3CN)$_6$]$^{2+}$ which could react with O_2^- to form the observed products or the O_2^- could attack [(pz_2TTP)Mn(CH_3CN)$_3$]$^{2+}$ prior to ligand redistribution. Alternatively, and more likely, considering the low energy edge of absorption bands (observed or calculated) and the redox behaviour, the excited state redox potentials of every species in the series [(pz_2TTP)Mn(CO)$_n$(CH_3CN)$_{3-n}$]$^+$ (n = 0 to 3) are predicted to be sufficiently negative (<−1.9 V *vs.* NHE) to reduce oxygen directly. Thus, photooxidation of the manganese(I) complexes might precede CO loss. Our group is continuing to investigate the photoreductive properties of carbonylmanganese complexes and will report our findings in due course.

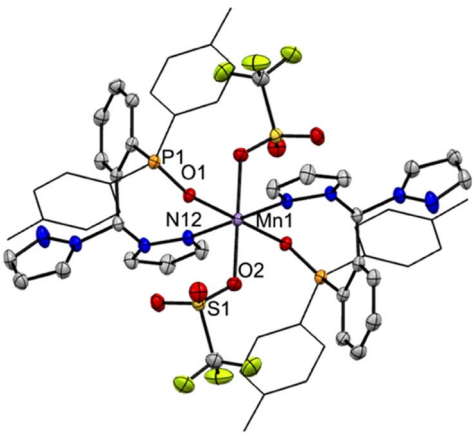

Fig. 8 Structure of *trans*-[Mn(κ^2NO-pz_2TTPO)$_2$(κ^1O-OTf)$_2$], **4**, from single crystal X-ray diffraction. Ellipsoids are drawn at the 50% probability level. Selected bond distances (Å): Mn1–O1 2.1169(10), Mn1–O2 2.2019(11), Mn1–N12 2.3511(14), P1–O1 1.5038(11), S2–O2 1.4571(12); selected bond angles (°): O1–Mn1–O1 180.0, O2–Mn1–O2 180.0, N12–Mn1–N12 180.0, O1–Mn1–O2 88.88(4), O1–Mn1–O2′ 91.12(4), O1–Mn1–N12 94.84(4), O1–Mn1–N12′ 85.16(4), O2–Mn1–N12 86.31(5), O2 Mn1 N12 93.69(5).

Experimental

Materials and methods

The ligand pz_2TTP was prepared by the literature route.[44] $Mn(CO)_5Br$ was used as received from Ambeed whereas $Re(CO)_5Br$ was prepared from commercial $Re_2(CO)_{10}$ (Pressure Chemical) by a literature procedure.[72] The complex [*fac*-$Mn(CO)_3(NCCH_3)_3$](O_3SCF_3) was prepared by a literature route from $Mn(CO)_5Br$ and AgO_3SCF_3 (Alfa Aesar) in CH_3CN.[73] Anhydrous Me_3NO was prepared from the commercial hydrate (TCI AMERICA) by recrystallization from hot dmf.[74] Tl(O_3SCF_3) was used as received from Sigma Aldrich. It is noted that thallium reagents are highly toxic and extra precautions are required for their safe handling and disposal in accord with local regulations. Midwest MicroLab, LLC, Indianapolis, Indiana 45250, performed all elemental analyses. Melting point determinations were made on samples contained in glass capillaries using an Electrothermal 9100 apparatus and are uncorrected. IR spectra were recorded on solid samples using a Thermo Scientific Nicolet iS5 IR spectrometer equipped with an iD3 Attenuated Total Reflection (ATR) accessory. ^{1}H, ^{13}C, ^{19}F, and ^{31}P NMR spectra were recorded on a Varian 400 MHz spectrometer. Chemical shifts were referenced to solvent resonances at δ_H 7.26 and δ_C 77.23 ppm for $CDCl_3$, δ_H 1.94 and δ_C 1.32 for CD_3CN, or by using external standards δ_F = 0.00 ppm for $CFCl_3$ or δ_P = 0.00 ppm for H_3PO_4 (aq). Abbreviations for NMR and UV-vis: br (broad), sh (shoulder), m (multiplet), ps (pseudo), s (singlet), d (doublet), t (triplet), q (quartet), p (pentet), sept (septet). Electronic absorption (UV-vis/NIR) measurements of solutions were made on an Agilent 8453 Diode array or a Cary 5000 spectrometer. Electrochemical measurements were collected under a nitrogen atmosphere for samples as 0.1 mM solutions in CH_3CN with 0.1 M NBu_4PF_6 as the supporting electrolyte. A three-electrode cell comprised of an Ag/AgCl electrode (separated from the reaction medium with a semipermeable polymer membrane filter), a platinum working electrode, and a glassy carbon counter electrode was used for the voltammetric measurements. Data were collected at scan rates of 50, 100, 200, 300, 400, and 500 mV s^{-1}. With this set up, the ferrocene/ferrocenium couple matched the literature value[75,76] with $E_{1/2}$ = +0.43 V in CH_3CN at a scan rate of 200 mV s^{-1}.

Crystallography

Single crystal X-ray intensity data from a colourless prism of **1**, a light yellow irregular block of **2-Mn**, a colourless block of **2-Re**, a yellow plate of **3-$Mn_{0.84}$·2-$Mn_{0.16}$**, a colourless plate of **3-Re**, and a colourless block of **4** were each collected at 100.0(1) K with an Oxford Diffraction Ltd. Supernova diffractometer equipped with a 135 mm Atlas CCD detector using Cu(Kα) radiation. Raw data frame integration and Lp corrections were performed with CrysAlisPro (Rigaku Oxford Diffraction, Ltd).[77] Final unit cell parameters were determined by least-squares refinement of 12 870, 13 074, 14 655, 12 814, 12 601, and 11 411 reflections of **1**, **2-Mn**, **2-Re**, **3-$Mn_{0.84}$·2-$Mn_{0.16}$**, **3-Re**, and **4** respectively, with $I > 2\sigma(I)$ for each. Analysis of the data showed negligible crystal decay during collection in each case. Direct methods structure

solutions, difference Fourier calculations and full-matrix least-squares refinements against F^2 were performed with SHELXTL.[78] Numerical absorption corrections based on Gaussian integration over a multifaceted crystal model were applied to the data for each of the complexes as implemented in the SCALE3 ABSPACK scaling algorithm.[79] All non-hydrogen atoms were refined with anisotropic displacement parameters with the exception of the minor disorder component CO atoms (20% occupancy) that overlay the Br atom of the major disorder component (80% occupancy) in the structure of **1**. Hydrogen atoms were placed in geometrically idealized positions and included as riding atoms. It is also noted that in the structure of **3-Mn$_{0.84}$·2-Mn$_{0.16}$** the triflate ion (C14 F1 F2 F3 S3 O3 O4 O5) is most likely disordered across two sites. The careful inspection has revealed the highest *Q* peak is 0.5 electrons. Modelling such disorder would require heavy restraints due to the low density available. Therefore, we have decided not to model this disorder because no other valuable information would be gained by doing so.

Single crystals of **3-Mn$_{0.92}$·2-Mn$_{0.08}$** were grown by vapor diffusion of diethyl ether into acetonitrile at ambient temperature in a closed vial. A small specimen was retrieved, placed on a microscope slide, coated in inert oil, mounted on a MiTeGen Dual Thickness MicroMount and placed on a goniometer head under a cold stream of N_2 gas. Data were collected at 100(2) K on a Bruker D8 Venture 4-circle diffractometer coupled to a Photon III C14 CMOS area detector with Cu Kα radiation ($\lambda = 1.54184$ Å) provided by a Incoatec IμS 3.0 micro-focus Cu X-ray source running at 50.0 kV and 1.1 mA. All data manipulations for **3-Mn$_{0.92}$·2-Mn$_{0.08}$** were carried out using the Bruker APEX-5 Software Suite.[80] Data were reduced, correcting for absorption, using the program SADABS.[81] Space group assignment was done using XPREP within the SHELXTL suite of programs.[82] Using the ShelXle graphical interface, the structure was solved by dual space methods employed by ShelXT and refined by full-matrix least-squares methods against F^2 using ShelXL with scattering factors and anomalous dispersion terms taken from the literature.[78] All non-hydrogen atoms not apparent from the initial solution were found from difference Fourier maps, and all heavy atoms were refined anisotropically. Special details for **3-Mn$_{0.92}$·2-Mn$_{0.08}$**. The initial refinement of the structure determined there was additional electron density around the CH_3CN molecule (N1 C15 C16), this was initially ignored as it was less than 10% contribution. After further consideration, we have decided to model this additional density as partially occupied CO. The occupancies of both the CO and CH_3CN were constrained to a sum of 1 and refined to 0.923(4) for the major component (N1 C15 C16) and 0.077(4) for the minor component (C10 O10). SADI was used for C10 and O10 to keep the bonding appropriate. Additionally, C10 and O10 of the CO molecule and N1 of the CH_3CN had their displacement parameters constrained with EADP. Further investigation has determined that the triflate molecule (C14 F1 F2 F3 S3 O3 O4 O5) was disordered across two sites. The occupancies of both components were constrained to a sum of 1 and refined to 0.72(2) for the major component (C14 F1 F2 F3 S3 O3 O4 O5) and 0.28(2) for the minor component (C14A F1A F2A F3A S3A O3A O4A O5A). The minor component was further restrained with SIMU and RIGU. All hydrogen atoms were placed in calculated positions and had their thermal parameters tied to the isotropic thermal parameters of the atoms to which they were bonded (1.5× for methyl, 1.2× for others).

The X-ray crystallographic parameters and further details of data collection and structure refinements are given in Table S1 of the ESI.† CCDC 2371547, 2371549–2371553, and 2383876 contains crystallographic information files. The powder X-ray diffraction (PXRD) patterns were collected at 295 K with a Rigaku MiniFlex II instrument using Cu Ka (1.54178 Å) radiation or at 100 K (for analysis of photolysis products) by using the Oxford Diffraction Ltd instrument.

Synthetic procedures

[(pz$_2$TTP)Re(CO)$_3$Br], 1. A mixture of 0.228 g (0.522 mmol) pz$_2$TTP and 0.212 g (0.522 mmol) $Re(CO)_5Br$ in 20 mL toluene was heated at reflux 16 h. Solvent was then removed from the resulting colourless solution by vacuum distillation leaving a white solid that was washed with two 5 mL portions Et_2O to remove trace free ligand and give 0.248 g (73% yield) of **1**. The solid was redissolved in 10 mL toluene, layered with 65 mL hexanes and solvents were allowed to diffuse overnight. The resulting X-ray quality colourless prisms (0.153 g, 62% yield) were collected by filtration dried by heating at 80 °C under vacuum 1 h to remove trace toluene. Anal. Calcd (found) for $C_{30}H_{25}BrN_4O_3PRe$: C, 45.81 (45.94); H, 3.20 (3.02); N, 7.12 (7.05). ^{1}H NMR (400 MHz, CD_3CN): δ_H (major component of mixture, see Fig. S2†) = 8.80 (dd, $J = 7.7$, 4 Hz, 1H, Ar), 8.63 (d, $J = 3.3$ Hz, 1H, H_5pz^A), 8.48 (d, $J = 2.5$ Hz, 1H, H_5pz^B), 8.10 (d, $J = 1.6$ Hz, 1H, H_3pz^A), 7.79 (d, $J = 1.1$ Hz, 1H, H_3pz^B), 7.60 (pst, $J = 7.7$ Hz, 1H, Ar), 7.42–7.23 (br m, 10H, tolyl, Ar, and H_{meth}), 6.79 (pst, $J =$ 10 Hz, 1H, Ar), 6.47 (dd, $J = 3$, 2 Hz, 1H, H_4pz^A), 6.26 (dd, $J = 2$, 1 Hz, 1H, H_4pz^A), 2.42 (s, 3H, tolyl-CH_3), 2.41 (s, 3H, tolyl-CH_3) ppm. ^{1}H NMR (400 MHz, CD_2Cl_2): δ_H (major component of mixture, see Fig. S2†) = 8.80 (dd, $J = 8$, 4 Hz, 1H, Ar), 8.71 (d, $J =$ 3 Hz, 1H, H5pz^A), 8.56 (d, $J = 2$ Hz, 1H, H_5pz^B), 7.97 (d, $J =$ 1.2 Hz, 1H, H_3pz^A), 7.76 (d, $J = 1.1$ Hz, 1H, H_3pz^B), 7.55 (pst, $J =$ 8 Hz, 1H, Ar), 7.42 (pst, $J = 10$ Hz, 1H, Ar), 7.36–7.23 (br m, 11H, tolyl and H_{meth}), 6.79 (dd, $J = 10$, 8 Hz, 1H, Ar), 6.40 (dd, $J = 3$, 2 Hz, 1H, H_4pz^A), 6.19 (dd, $J = 2$, 1 Hz, 1H, H_4pz^A), 5.33 (s, 4H, CH_2Cl_2), 2.45 (s, 6H, tolyl-CH_3) ppm. ^{31}P NMR (162 MHz, CD_3CN): $\delta_P = 10.2$ (s, 1P, major isomer), 0.3 (s, 0.3P, minor isomer) ppm. ^{31}P NMR (162 MHz, CD_2Cl_2): $\delta_P = 10.7$ (s, 1P, major isomer), 0.7 (s, 0.3P, minor isomer) ppm.

[(pz$_2$TTP)Re(CO)$_3$][O$_3$SCF$_3$], 2-Re. A mixture of 0.609 g (1.50 mmol) $Re(CO)_5Br$, 0.650 g (1.50 mmol) pz$_2$TTP, and 0.530 g (1.50 mmol) TlOTf in 20 mL CH_3CN was heated at reflux 16 h. The precipitate of TlBr was removed by filtration. Solvent was removed from the filtrate to leave a colourless solid that was washed with two 5 mL portions Et_2O and dried under vacuum to give 1.23 g (96% yield) of **2-Re** as a colourless powder. Anal. Calcd (found) for $C_{31}H_{25}F_3N_4O_6PSRe$: C, 43.51 (43.12); H, 2.94 (2.94); N, 6.55 (6.59). ^{1}H NMR (400 MHz, CD_3CN): $\delta_H = 8.29$ (s, 1H, H_{meth}), 8.26 (d, $J = 2.5$ Hz, 2H, H_5pz), 8.07 (d, $J = 1.6$ Hz, 2H, H_3pz), 7.92 (dd, $J = 7.7$, 7.4 Hz, 1H, *o*-tolyl), 7.67 (pst, $J_{app} =$

7.7 Hz, 1H, *o*-tolyl), 7.43 (pst, J_{app} = 7.7 Hz, 1H, *o*-tolyl), 7.29 (dd, J = 8.2, 1.2 Hz, 4H, H_m-*p*-tolyl), 7.10 (m, 5H, *p*-tolyl and *o*-tolyl), 6.58 (dd, J = 2.5, 1.6 Hz, 2H, H_4pz), 2.39 (s, 6H, CH_3) ppm. ^{13}C NMR (101 MHz, CD_3CN): δ_c = 150.7 (s, C_4tol), 142.8 (d, J = 2 Hz, C_3pz), 140.5 (d, J = 14.0 Hz), 139.4 (d, J = 1.3 Hz), 137.4 (s, C_5pz), 134.0 (d, J = 2.0 Hz), 133.3 (d, J = 11.5 Hz), 133.0 (d, J = 8.1 Hz), 132.8 (d, J = 5.8 Hz), 130.7 (d, J = 10.8 Hz), 130.6 (d, J = 33 Hz, $C_1^{Ar\ or\ tol}$), 128.9 (q, J = 52 Hz, CF_3), 113.5, 110.9 (C_4pz), 78.2 (C_{meth}), 21.3 (CH_3) ppm; CO's not observed. ^{19}F NMR (367 MHz, CD_3CN): δ_F = −79.3 (s, 3 F) ppm. ^{31}P NMR (162 MHz, CD_3CN): δ_P = 4.5 ppm. X-ray quality crystals were grown by dissolving 0.351 g of **2-Re** in 16 mL acetone, then layering with 64 mL hexanes and allowing solvents to diffuse 24 h whereupon 0.263 g of colourless rectangular prisms were isolated by filtration and drying under vacuum.

[(pz_2TTP)Mn(CO)$_3$](O_3SCF_3), 2-Mn. In a foil-covered flask, a mixture of 0.650 g (1.50 mmol) [Mn(CO)$_3$($NCCH_3$)$_3$](O_3SCF_3) and 0.617 g (1.50 mmol) pz_2TTP in 20 mL CH_3CN was stirred at room temperature for 2 h. Solvent was removed from the resulting yellow solution, and the yellow residue was washed with two 5 mL portions Et_2O, then dried under vacuum to give 0.948 g (89% yield) of **2-Mn** as a yellow powder. Anal. Calcd (found) for $C_{31}H_{25}F_3N_4O_6PSMn$: C, 51.39 (51.15); H, 3.48 (3.53); N, 7.73 (7.90). ^{1}H NMR (400 MHz, CD_3CN): δ_H = 8.27 (br s, 2H, H_5pz), 8.08 (s, 1H, H_{meth}), 8.02 (br s, 2H, H_3pz), 7.83 (br dd, J = 7.7, 7.0 Hz, 1H, *o*-tolyl), 7.59 (pst, J_{app} = 7.4 Hz, 1H, *o*-tolyl), 7.35 (pst, J_{app} = 7.4 Hz, 1H, *o*-tolyl), 7.26 (br d, J = 7.0 Hz, 4H, H_m-*p*-tolyl), 7.10 (m, 5H, *p*-tolyl and *o*-tolyl), 6.63 (br s, 2H, H_4pz), 2.36 (s, 6H, CH_3) ppm. ^{13}C NMR (101 MHz, CD_3CN): δ_c = 219.3, 213.8, 150.3, 142.6, 140.8 (d, J = 14.4 Hz), 139.5, 137.9, 133.7, 133.3 (d, J = 10.5 Hz, tolyl), 132.5 (d, J = 3.4 Hz), 132.1 (d, J = 7.8 Hz), 131.1 (d, J = 21.3 Hz), 130.6 (d, J = 10.1 Hz), 128.9 (q, J = 45.0 Hz, CF_3), 111.0 (d, J = 7.8 Hz), 110.9 (C_4pz), 76.9 (C_{meth}), 21.3 (CH_3) ppm. ^{19}F NMR (367 MHz, CD_3CN): δ_F = −79.1 (s, 3F) ppm. ^{31}P NMR (162 MHz, CD_3CN): δ_P = 33.8, ppm. X-ray quality crystals were grown by dissolving 0.048 g of **2-Mn** in 2 mL CH_2Cl_2, layered with 6 mL hexanes and solvents were allowed to diffuse 24 h whereupon 0.045 g of yellow crystals were isolated by filtration and drying under vacuum.

[(pz_2TTP)Re(CO)$_2$($NCCH_3$)(O_3SCF_3)], 3-Re. A mixture of 0.879 g (1.03 mmol) of **2-Re** and 0.0771 g (1.03 mmol) Me_3NO in 20 mL CH_3CN was heated at reflux under argon for 12 h. After the solvent was removed from the resulting colourless solution under vacuum, the crude material was washed with two 2 mL portions Et_2O and dried under vacuum to give 0.890 g (99% yield) of **3-Re** as a colourless solid. The solid was then dissolved in 20 mL acetone, filtered through a small Celite plug, then layered with 60 mL hexanes and solvents were allowed to diffuse 16 h whereupon 0.563 g (63% yield) of colourless rectangular prisms were isolated by filtration and drying under vacuum. Anal. Calcd (found) for $C_{32}H_{29}F_3N_5O_{5.5}PSRe$, **3-Re**·0.5 H_2O: C, 43.78 (43.79); H, 3.33 (3.08); N, 7.98 (7.71). ^{1}H NMR (400 MHz, CD_3CN): δ_H = 8.16 (d, J = 2.4 Hz, 2H, H_5pz), 8.15 (s, 1H, H_{meth}), 7.97 (d, J = 1.7 Hz, 2H, H_3pz), 7.85 (br dd, J = 7, 5.6), 7.60 (pst, J_{app} = 7.7 Hz, 1H, *o*-tol), 7.37 (pst, J_{app} = 7.7 Hz, 1H, *o*-tol), 7.21 (d, J = 8.1 Hz, 4H, *p*-tolyl), 7.04 (dd, J = 11.0, 8.1 Hz, 4H, *p*-tolyl), 6.98 (dd, J = 10.6, 7.7, 1H, *o*-tolyl), 6.51 (dd, J = 2.4, 1.7, 2H, H_4pz), 2.37 (s, 6H, CH_3-*p*-tolyl), 2.23 (s, 3H, CH_3CN) ppm. ^{13}C NMR (101 MHz, CD_3CN): δ_c = 200.2 (d, J = 7 Hz, CO), 148.7, 141.6, 140.5 (d, J = 13.5 Hz), 138.3, 133.4 (d, J = 4.4 Hz), 133.2 (d, J = 10.9 Hz), 133.1 (d, J = 8.2 Hz), 133.0 (d, J = 2 Hz), 132.8, 132.1 (d, J = 5.7 Hz), 130.4, 130.0 (d, 10.7 Hz), 111.0, 110.2, 78.6, 21.2, 3.9 ppm. ^{19}F NMR (367 MHz, CD_3CN): δ_F = −79.2 (s, 3F) ppm. ^{31}P NMR (162 MHz, CD_3CN): δ_P = 17.9 (s, 1P) ppm.

[(pz_2TTP)Mn(CO)$_2$($NCCH_3$)(O_3SCF_3)], 3-Mn. In a foil-covered flask, a mixture of 0.500 g (0.690 mmol) of **2-Mn** and 0.0518 g (0.690 mmol) of Me_3NO in 20 mL CH_3CN was stirred at room temperature for 2 h while dynamically purging any evolved NMe_3 with a steady flow of argon. Solvent was removed from the resulting yellow orange solution, and the yellow residue was washed with two 5 mL portions Et_2O and dried under vacuum to give 0.500 g (98% yield) as a yellow-orange powder. Anal. Calcd (found) for $C_{32.5}H_{29}F_3ClN_5O_5PSMn$, **3-Mn**·0.5$CH_2Cl_2$: C, 51.58 (51.80); H, 3.75 (3.89); N, 8.98 (8.88). ^{1}H NMR (400 MHz, CD_3CN): δ_H = 8.28 (s, 2H, H_5pz), 8.19 (s, 1H, H_{meth}), 8.12 (s, 2H, H_3pz), 7.85 (m, 1H, Ar), 7.53 (pst, J = 7 Hz, 1H, Ar), 7.26 (pst, J = 8 Hz, 1H, Ar), 7.17 (m, 4H, tolyl), 6.99 (m, 4H, tolyl), 6.93 (pst, J = 8 Hz, Ar), 6.59 (s, 2H, H_4pz), 2.32 (s, 6H, tol-CH_3), 1.96 (s, 3H, CH_3CN) ppm. ^{13}C NMR (101 MHz, CD_3CN): δ_c = 150.3, 142.6, 140.2, 139.6, 137.9, 134.5 (d, J = 17 Hz), 133.7, 133.3 (d, J = 10.5 Hz), 132.6 (d, J = 4.6 Hz), 132.0 (d, J = 8.2 Hz), 130.6 (d, J = 10.5 Hz), 130.3 m, 130.2 (q, J = 45 Hz, CF_3), 111.0, 77.1. 21.3, 14.2 ppm; CO's not observed. ^{19}F NMR (367 MHz, CD_3CN): δ_F = −79.3 (s, 3F) ppm. ^{31}P NMR (162 MHz, CD_3CN): δ_P = 66.3 (s, 1P) ppm. Crystals of **3-Mn** unsuitable for single crystal X-ray diffraction can be made by dissolving the crude 0.149 g of impure **3-Mn** in 2 mL CH_2Cl_2, layering with 8 mL hexanes, and allowing solvents to diffuse 15 h whereupon 0.120 g (81% recovery) of yellow-orange crystals were collected after filtration and drying under vacuum. If such crystals are only air-filtered they analysed as: $C_{34.25}H_{33}F_3Cl_{1.5}N_5O_5PSMn$, **3-Mn**·0.75$CH_2Cl_2$·0.25$C_6H_{14}$: C, 50.00 (49.72); H, 4.04 (3.74); N, 8.51 (8.64). X-ray quality crystals of general composition **3-Mn**$_{(1-x)}$·**2-Mn**$_x$ (x = 0.08–0.30) can be grown from impure samples during an attempted syntheses with sub-stoichiometric amounts of $ONMe_3$ or its hydrate by using either CH_2Cl_2 as a solvent by layering the filtered product mixture with hexanes or using CH_3CN as solvent and subjecting to vapor diffusion with Et_2O.

Photoinduced CO release

Manganese complexes. A borosilicate vial was charged with 10 mL of a CH_3CN solution that was 2.5 mM in **2-Mn** or **3-Mn**. The flask was placed in a photoreactor 15 cm from a 50 W 390 nm LED light source. During irradiation, 1 mL aliquots were removed and passed through a 0.5 × 1.0 cm Celite filter to remove any insoluble impurities with care taken to avoid further light exposure. A 20 μL portion of the filtered solution was used for immediate ATR-IR analysis. For electronic absorption analysis, 0.2 mL of filtered solution was diluted to 10 mL and spectra was recorded.

Rhenium complexes. A standard 1 cm path length quartz fluorescence cuvette, was charged with 1.0 mL of a CH_3CN or CD_3CN solution that was 0.020–0.035 M in **2-Re** or **3-Re**. After

the cuvette was positioned 19 cm from a 38 W UV-C lamp (254 nm), the photoreactor was closed (Caution: UV-C irradiation is harmful to living organisms, minimize exposure) and then the sample was irradiated. The temperature inside the reactor was monitored during irradiation *via* a thermocouple and never exceeded 25.8 °C. The photoirradiation was interrupted in regular time intervals to take spectroscopic measurements. For IR studies, 20 μL aliquots of the reaction solution were used directly.

Computational methods

General considerations. DFT calculations were performed using Gaussian 16 (ref. 83) with M06L meta-hybrid GGA functional[84] that has been found to be useful for affording accurate solutions to a wide variety of computation problems at low computational expense and notably include relativistic effects.[85] Geometry optimizations used the combination of the M06L functional and the def2-TZVP triple-zeta basis set.[86,87] Solvent (acetonitrile) effects were accounted for by using the polarizable continuum model IEFPCM.[88] Analytical vibrational frequency calculations were carried out to verify that optimized geometries were stationary points. Time-dependent DFT methodology was used for excitation energy calculations.[89–91] The calculation of reduction potentials followed Truhlar's methodology[92] and used recommendations outlined by Rulíšek.[93]

Conclusions

The soft C-heteroscorpionate ligand, pz_2TTP, binds to rhenium(I) and manganese(I) carbonyl centres in the expected κ^3PN_2-mode. However, with rhenium(I) the more unusual κ^2PN-binding mode has also been found, where the hemilabile pyrazolyl arm dissociates to accommodate metal-ion binding. For $[(\kappa^3PN_2\text{-}pz_2TTP)M(CO)_3](OTf)$, **2-M**, the CO stretching frequencies indicated a relative donor strength that is intermediate between the traditional C-scorpionate Tpm with an N_3-donor set and the anionic hard-heteroscorpionate (bpza) – with an N_2O donor set. The electrochemical data of **2-M** show that pz_2TTP ligand stabilized the univalent state by about 100 mV relative to the Tpm derivative and *ca.* 500 mV compared to related complexes with anionic scorpionates. The phosphorous donor of pz_2TTP labilizes the *trans*-CO giving *cis*-$[(\kappa^3PN_2\text{-}pz_2TTP)Mn(CO)_2(CH_3CN)](OTf)$, **3-Mn** simply on heating in CH_3CN ($t_{1/2}$ = 15 min). The rhenium analogue **3-Re** is formed exceedingly slowly from **2-Re** under these conditions, so is better prepared by decarboxylation with $ONMe_3$. Despite **3-M** having stronger M–C bonds than **2-M** from IR and single crystal X-ray diffraction data, the **3-M** species are more reactive due to two factors. First, **3-M** substantially more electron rich than their **2-M** counterparts by about 600 mV due to replacement of CO with the poorer π-acceptor CH_3CN. Second, the MLCT bands in **3-M** are broadened and red-shifted relative to **2-M**, increasing their visible light sensitivity. Irradiation of either **2-M** or **3-M** at their MLCT bands causes total loss of CO over the course of 20 min for Mn derivatives but days for Re compounds. A monocarbonyl was never detected by IR or NMR spectroscopy for either metal. It is likely that, if formed, such species would be even more electron rich and photoreactive than **3-M**. The photoreducing properties of **2-Mn** were demonstrated by the isolation of $[Mn^{II}(\kappa^2NO\text{-}pz_2TTPO)_2(\kappa^1O\text{-}OTf)_2]$, **4**, (and manganese oxides) during photoirradiation under atmospheric conditions, a result of oxygen activation. The potential photoreductive properties of pz_2TTP and other scorpionate complexes of $M(CO)_3^+$ in organic syntheses warrant further investigation.

Data availability

The data supporting this article have been included as part of the ESI.† This data also includes crystallographic data which have been deposited at the CCDC with numbers 2371547, 2371549–2371553 and 2383876, and can be obtained free of charge from **https://www.ccdc.cam.ac.uk/structures**.

Author contributions

JRG was responsible for conceptualizing, supervising, project administration, contributing to writing the original draft, reviewing, and editing subsequent drafts. JPV was responsible for investigation, data curation, formal analysis, and contributed to writing the original draft, reviewing, and editing subsequent drafts. ANE performed and reviewed diffraction experiments and reviewed and edited manuscript drafts.

Conflicts of interest

There are no conflicts to declare.

Acknowledgements

JRG thanks Marquette University for financial support. This research was funded in part by the National Science foundation award CNS-1828649 "MRI: Acquisition of iMARC: High Performance Computing for STEM Research and Education in Southeast Wisconsin". Crystal data for (CCDC 2383876) was collected at the Marquette University Diffraction Facility with funding for the Bruker D8 Venture diffractometer provided by NSF Award CHE-2320762.

Notes and references

1 S. Weber and K. Kirchner, Manganese Alkyl Carbonyl Complexes: From Iconic Stoichiometric Textbook Reactions to Catalytic Applications, *Acc. Chem. Res.*, 2022, **55**, 2740–2751.
2 K. Das, S. Waiba, A. Jana and B. Maji, Manganese-catalyzed hydrogenation, dehydrogenation, and hydroelementation reactions, *Chem. Soc. Rev.*, 2022, **51**, 4386–4464.
3 A. Mukherjee and D. Milstein, Homogeneous Catalysis by Cobalt and Manganese Pincer Complexes, *ACS Catal.*, 2018, **8**, 11435–11469.
4 S. Hostachy, C. Policar and N. Delsuc, Re(I) carbonyl complexes: Multimodal platforms for inorganic chemical biology, *Coord. Chem. Rev.*, 2017, **351**, 172–188.

5 Y. Kuninobu and K. Takai, Organic Reactions Catalyzed by Rhenium Carbonyl Complexes, *Chem. Rev.*, 2011, **111**, 1938–1953.
6 P. R. Elowe, N. M. West, J. A. Labinger and J. E. Bercaw, Transformations of Group 7 Carbonyl Complexes: Possible Intermediates in a Homogeneous Syngas Conversion Scheme, *Organometallics*, 2009, **28**, 6218–6227.
7 C. C. Konkankit, S. C. Marker, K. M. Knopf and J. J. Wilson, Anticancer activity of complexes of the third row transition metals, rhenium, osmium, and iridium, *Dalton Trans.*, 2018, **47**, 9934–9974.
8 K. Schindler and F. Zobi, Anticancer and Antibiotic Rhenium Tri- and Dicarbonyl Complexes: Current Research and Future Perspectives, *Molecules*, 2022, **27**, 539.
9 R. Alberto, Role of Pure Technetium Chemistry: Are There Still Links to Applications in Imaging?, *Inorg. Chem.*, 2023, **62**, 20539–20548.
10 J. Marhenke, K. Trevino and C. Works, The chemistry, biology and design of photochemical CO releasing molecules and the efforts to detect CO for biological applications, *Coord. Chem. Rev.*, 2016, **306**, 533–543.
11 U. Schatzschneider, PhotoCORMs: Light-triggered release of carbon monoxide from the coordination sphere of transition metal complexes for biological applications, *Inorg. Chim. Acta*, 2011, **374**, 19–23.
12 E. Kottelat and Z. Fabio, Visible Light-Activated PhotoCORMs, *Inorganics*, 2017, **5**, 24.
13 T. T. Tien Vo, Q. C. Vo, V. P. Tuan, Y. Wee, H.-C. Cheng and I.-T. Lee, The potentials of carbon monoxide-releasing molecules in cancer treatment: An outlook from ROS biology and medicine, *Redox Biol.*, 2021, **46**, 102124.
14 M. A. Andrade and L. M. D. R. S. Martins, Novel Chemotherapeutic Agents – The Contribution of Scorpionates, *Curr. Med. Chem.*, 2019, **26**, 7452–7475.
15 R. Weinstain, T. Slanina, D. Kand and P. Klán, Visible-to-NIR-Light Activated Release: From Small Molecules to Nanomaterials, *Chem. Rev.*, 2020, **120**, 13135–13272.
16 M. A. Wright and J. A. Wright, PhotoCORMs: CO release moves into the visible, *Dalton Trans.*, 2016, **45**, 6801–6811.
17 A. J. Kosanovich, W.-C. Shih and O. V. Ozerov, Synthesis and characterization of unsaturated Manganese(I) and Rhenium(I) dicarbonyl complexes supported by an anionic PNP pincer, *J. Organomet. Chem.*, 2019, **897**, 1–6.
18 T. B. Gunnoe, M. Sabat and W. D. Harman, Reactions of $TpRe(CO)_2(THF)$ with Aromatic Molecules (Tp = Hydridotris(pyrazolyl)borate), *J. Am. Chem. Soc.*, 1998, **120**, 8747–8754.
19 R. G. Bergman, T. R. Cundari, A. M. Gillespie, T. B. Gunnoe, W. D. Harman, T. R. Klinckman, M. D. Temple and D. P. White, Computational Study of Methane Activation by $TpRe(CO)_2$ and $CpRe(CO)_2$ with a Stereoelectronic Comparison of Cyclopentadienyl and Scorpionate Ligands, *Organometallics*, 2003, **22**, 2331–2337.
20 D. M. Tellers, S. J. Skoog, R. G. Bergman, T. B. Gunnoe and W. D. Harman, Comparison of the Relative Electron-Donating Abilities of Hydridotris(pyrazolyl)borate and Cyclopentadienyl Ligands: Different Interactions with Different Transition Metals, *Organometallics*, 2000, **19**, 2428–2432.
21 D. Álvarez, M. I. Menéndez and R. López, Computational Design of Rhenium(I) Carbonyl Complexes for Anticancer Photodynamic Therapy, *Inorg. Chem.*, 2022, **61**, 439–455.
22 K. Schindler, A. Crochet and F. Zobi, Aerobically stable and substitutionally labile α-diimine rhenium dicarbonyl complexes, *RSC Adv.*, 2021, **11**, 7511–7520.
23 A. Otero, J. Fernández-Baeza, A. Lara-Sánchez, J. Tejeda and L. F. Sánchez-Barba, Recent Advances in the Design and Coordination Chemistry of Heteroscorpionate Ligands Bearing Stereogenic Centres, *Eur. J. Inorg. Chem.*, 2008, **2008**, 5309–5326.
24 S. Trofimenko, Recent advances in poly(pyrazolyl)borate (scorpionate) chemistry, *Chem. Rev.*, 1993, **93**, 943–980.
25 A. Otero, J. Fernández-Baeza, A. Lara-Sánchez and L. F. Sánchez-Barba, Metal complexes with heteroscorpionate ligands based on the bis(pyrazol-1-yl) methane moiety: Catalytic chemistry, *Coord. Chem. Rev.*, 2013, **257**, 1806–1868.
26 C. Pettinari and R. Pettinari, Metal derivatives of poly(pyrazolyl)alkanes: II. Bis(pyrazolyl)alkanes and related systems, *Coord. Chem. Rev.*, 2005, **249**, 663–691.
27 L. M. D. R. S. Martins, C-scorpionate complexes: Ever young catalytic tools, *Coord. Chem. Rev.*, 2019, **396**, 89–102.
28 C. Pettinari, *Scorpionates II: Chelating Borate Ligands*, Imperial College Press, London, 2008.
29 S. Pai, M. Hafftlang, G. Atongo, C. Nagel, J. Niesel, S. Botov, H.-G. Schmalz, B. Yard and U. Schatzschneider, New modular manganese(I) tricarbonyl complexes as PhotoCORMs: *in vitro* detection of photoinduced carbon monoxide release using COP-1 as a fluorogenic switch-on probe, *Dalton Trans.*, 2014, **43**, 8664–8678.
30 D. L. Reger, J. R. Gardinier, T. C. Grattan and M. D. Smith, Tricarbonylmanganese(I) derivatives of [Di(pyrazolyl)(2-pyridyl)methyl]aryl scorpionates, *J. Organomet. Chem.*, 2005, **690**, 1901–1912.
31 J. R. Gardinier, K. J. Meise, F. Jahan and S. V. Lindeman, Reaction Chemistry of Silver(I) Trifluoromethanesulfonate Complexes of Nitrogen-Confused C-Scorpionates., *Inorg. Chem.*, 2018, **57**, 1572–1589.
32 E. Hübner, G. Türkoglu, M. Wolf, U. Zenneck and N. Burzlaff, Novel N, N,O Scorpionate Ligands and Transition Metal Complexes Thereof Suitable for Polymerisation, *Eur. J. Inorg. Chem.*, 2008, **2008**, 1226–1235.
33 W. Tzegai, M. Reil and N. Burzlaff, Bis(4-carboxylpyrazol-1-yl)acetic acid: a scorpionate ligand for complexes with improved water solubility, *Dalton Trans.*, 2022, **51**, 6839–6845.
34 N. Burzlaff, I. Hegelmann and B. Weibert, Bis(pyrazol-1-yl) acetates as tripodal "scorpionate" ligands in transition metal carbonyl chemistry: syntheses, structures and reactivity of manganese and rhenium carbonyl complexes of the type $[LM(CO)_3]$ (L = bpza, bdmpza), *J. Organomet. Chem.*, 2001, **626**, 16–23.
35 F. Strinitz, P. Trautner, H. Pfeiffer, U. Schatzschneider and N. Burzlaff, Synthesis and characterization of

heteroscorpionate-based manganese carbonyl complexes as CO-releasing molecules, *Tetrahedron*, 2015, **71**, 2951–2954.

36 E. Hübner, N. V. Fischer, F. W. Heinemann, U. Mitra, V. Dremov, P. Müller and N. Burzlaff, N, N,O Ligands Based on Triazoles and Transition Metal Complexes Thereof, *Eur. J. Inorg. Chem.*, 2010, **2010**, 4100–4109.

37 L. Peters, E. Hübner, T. Haas, F. W. Heinemann and N. Burzlaff, 3,3-Bis(3,5-dimethylpyrazol-1-yl)propionic acid: A tripodal *N*,*N*,*O* ligand for manganese and rhenium complexes – Syntheses and structures, *J. Organomet. Chem.*, 2009, **694**, 2319–2327.

38 G. Türkoglu, F. W. Heinemann and N. Burzlaff, Transition metal complexes bearing a 2,2-bis(3,5-dimethylpyrazol-1-yl) propionate ligand: one methyl more matters, *Dalton Trans.*, 2011, **40**, 4678–4686.

39 L. Peters, E. Hübner, T. Haas, F. W. Heinemann and N. Burzlaff, 3,3-Bis(3,5-dimethylpyrazol-1-yl)propionic acid: A tripodal *N*,*N*,*O* ligand for manganese and rhenium complexes – Syntheses and structures, *J. Organomet. Chem.*, 2009, **694**, 2319–2327.

40 C. Reus, K. Ruth, S. Tüllmann, M. Bolte, H.-W. Lerner, B. Weber, M. C. Holthausen and M. Wagner, Synthesis, Molecular Structure, and Physical Properties of the Complexes $[PhB(pz)_2(CH_2SMe)_2M]$ (M = Mn^{II}, Fe^{II}; pz = pyrazol-1-yl) Containing a Novel [N, N,S]-Heteroscorpionate Ligand, *Eur. J. Inorg. Chem.*, 2011, **2011**, 1709–1718.

41 T. Godau, F. Platzmann, F. W. Heinemann and N. Burzlaff, An enantiopure N, N,S scorpionate ligand derived from (+)-camphor, *Dalton Trans.*, 2008, 254–255.

42 H.-M. Berends and P. Kurz, Investigation of light-triggered carbon monoxide release from two manganese photoCORMs by IR, UV-vis and EPR spectroscopy, *Inorg. Chim. Acta*, 2012, **380**, 141–147.

43 U. Sachs, G. Schaper, D. Winkler, D. Kratzert and P. Kurz, Light- or oxidation-triggered CO release from $[Mn^{I}(CO)_3(\kappa^3\text{-}L)]$ complexes: reaction intermediates and a new synthetic route to $[Mn^{III/IV}{}_2(\mu\text{-}O)_2(L)_2]$ compounds, *Dalton Trans.*, 2016, **45**, 17464–17473.

44 J. R. Gardinier, J. S. Hewage and S. V. Lindeman, Isomer Dependence in the Assembly and Lability of Silver(I) Trifluoromethanesulfonate Complexes of the Heteroditopic Ligands, 2-, 3-, and 4-[Di(1H-pyrazolyl)methyl]phenyl(di-p-tolyl)phosphine, *Inorg. Chem.*, 2014, **53**, 12108–12121.

45 M. Abubekerov and P. L. Diaconescu, Synthesis and Characterization of Ferrocene-Chelating Heteroscorpionate Complexes of Nickel(II) and Zinc(II), *Inorg. Chem.*, 2015, **54**, 1778–1784.

46 M. Abubekerov, S. M. Shepard and P. L. Diaconescu, Switchable Polymerization of Norbornene Derivatives by a Ferrocene-Palladium(II) Heteroscorpionate Complex, *Eur. J. Inorg. Chem.*, 2016, **2016**, 2634–2640.

47 M. Y. Petyuk, A. S. Berezin, A. L. Gushchin, I. Y. Bagryanskaya, A. Y. Baranov and A. V. Artem'ev, Luminescent Re(I) scorpionates supported by tris(2-pyridyl) phosphine and its derivatives, *Inorg. Chim. Acta*, 2021, **516**, 120136.

48 D. H. Gibson, M. S. Mashuta and H.-Y. He, Tri-carbonyl-[1,1′,1″-ethylidyne-tris(pyrazole-κN^2)]-rhenium(I) bromide and tri-carbonyl-[methylidyne-tris-(pyrazole-κN^2)]-rhenium(I) iodide ethanol hemisolvate, *Acta Crystallogr., Sect. C: Cryst. Struct. Commun.*, 2001, **57**, 1135–1137.

49 P. C. Kunz, M. Berghahn, N. E. Brückmann, M. Dickmeis, M. Kettel and B. Spingler, Functionalised Tris(pyrazolyl) methane Ligands and $Re(CO)_3$ Complexes Thereof, *Z. Anorg. Allg. Chem.*, 2009, **635**, 471–478.

50 D. L. Reger, K. J. Brown and M. D. Smith, Rhenium tricarbonyl complexes of tris(pyrazolyl)methane ligands: first structural characterization of an isomer pair of tris(pyrazolyl)methane derivatives and the supramolecular structure of the homobimetallic complex $\{1,4\text{-}C_6H_4[CH_2OCH_2C(pz)_3]_2[Re(CO)_3]_2\}(Br)_2$, *J. Organomet. Chem.*, 2002, **658**, 50–61.

51 J. Niesel, A. Pinto, H. W. P. N'Dongo, K. Merz, I. Ott, R. Gust and U. Schatzschneider, Photoinduced CO release, cellular uptake and cytotoxicity of a tris(pyrazolyl)methane (tpm) manganese tricarbonyl complex, *Chem. Commun.*, 2008, 1798–1800.

52 D. L. Reger, T. C. Grattan, K. J. Brown, C. A. Little, J. J. S. Lamba, A. L. Rheingold and R. D. Sommer, Syntheses of tris(pyrazolyl)methane ligands and $\{[tris(pyrazolyl)methane]Mn(CO)_3\}SO_3CF_3$ complexes: comparison of ligand donor properties, *J. Organomet. Chem.*, 2000, **607**, 120–128.

53 M. Angaroni, G. A. Ardizzoia, G. D'Alfonso, G. L. Monica, N. Masciocchi and M. Moret, Photochemical reactions of tricarbonyl[hydrotris(1-pyrazolyl)borato]rhenium(I) in the presence of neutral donor ligands. X-Ray crystal structures of the substitution derivatives $[Re\{HB(pz)_3\}(CO)_2L]$, with L = C_4H_8O or PPh_3, *J. Chem. Soc., Dalton Trans.*, 1990, 1895–1900.

54 T. B. Gunnoe, M. Sabat and W. D. Harman, Reactions of $TpRe(CO)_2(THF)$ with Aromatic Molecules (Tp = Hydridotris(pyrazolyl)borate), *J. Am. Chem. Soc.*, 1998, **120**, 8747–8754.

55 P. Kurz, D. Rattat, D. Angst, H. Schmalle, B. Spingler, R. Alberto, H. Berke and W. Beck, The chemistry of the fac-$[Re(CO)_2(NO)]^{2+}$ fragment in aqueous solution, *Dalton Trans.*, 2005, 804–810.

56 A. J. Hallett, R. A. Baber, A. G. Orpen and B. D. Ward, The co-ordination chemistry of tris(3,5-dimethylpyrazolyl)methane manganese carbonyl complexes: Synthetic, electrochemical and DFT studies, *Dalton Trans.*, 2011, **40**, 9276–9283.

57 N. J. Stone, Table of nuclear magnetic dipole and electric quadrupole moments, *At. Data Nucl. Data Tables*, 2005, **90**, 75–176.

58 A. M. Camp, M. R. Kita, J. Grajeda, P. S. White, D. A. Dickie and A. J. M. Miller, Mapping the Binding Modes of Hemilabile Pincer–Crown Ether Ligands in Solution Using Diamagnetic Anisotropic Effects on NMR Chemical Shift, *Inorg. Chem.*, 2017, **56**, 11141–11150.

59 K. E. Aldrich, B. S. Billow, D. Holmes, R. D. Bemowski and A. L. Odom, Weakly Coordinating yet Ion Paired: Anion

Effects on an Internal Rearrangement, *Organometallics*, 2017, **36**, 1227–1237.

60 W. M. Ward, B. H. Farnum, M. Siegler and G. J. Meyer, Chloride Ion-Pairing with Ru(II) Polypyridyl Compounds in Dichloromethane, *J. Phys. Chem. A*, 2013, **117**, 8883–8894.

61 E. Kleinpeter, A. Koch, H. S. Sahoo and D. K. Chand, Anisotropic effect of the nitrate anion—manifestation of diamagnetic proton chemical shifts in the ^{1}H NMR spectra of NO_3^- coordinated complexes, *Tetrahedron*, 2008, **64**, 5044–5050.

62 H. S. Sahoo, D. K. Chand, S. Mahalakshmi, M. H. Mir and R. Raghunathan, Manifestation of diamagnetic chemical shifts of proton NMR signals by an anisotropic shielding effect of nitrate anions, *Tetrahedron Lett.*, 2007, **48**, 761–765.

63 A. Macchioni, Ion Pairing in Transition-Metal Organometallic Chemistry, *Chem. Rev.*, 2005, **105**, 2039–2074.

64 G. N. La Mar, Isotropic Shifts of Some Ionic Complexes of Cobalt(II) and Nickel(II) : Evidence for Ion Pairing, *J. Chem. Phys.*, 1964, **41**, 2992–2998.

65 J. Ammer, C. Nolte, K. Karaghiosoff, S. Thalmair, P. Mayer, R de Vivie-Riedle and H. Mayr, Ion-Pairing of Phosphonium Salts in Solution: C–H···Halogen and C–H···π Hydrogen Bonds, *Chem.–Eur. J.*, 2013, 14612–14630.

66 K. Wu, D. Mukherjee, A. Ellern, A. D. Sadow and W. E. Geiger, Anodic electrochemistry of Mn and Re tricarbonyl complexes of tris(oxazolinyl)phenyl borate ligands : comparison to tris(pyrazolyl) borate complexes, *New J. Chem.*, 2011, **35**, 2169–2178.

67 A. R. Schoenberg and W. P. Anderson, Photochemical reactions of poly(1-pyrazolyl)boratotricarbonylmanganese(I) with phosphorus donor ligands, *Inorg. Chem.*, 1972, **11**, 85–87.

68 M. E. Peover and B. S. White, Electrolytic reduction of oxygen in aprotic solvents: The superoxide ion, *Electrochim. Acta*, 1966, **11**, 1061–1067.

69 M. Hayyan, M. A. Hashim and I. M. AlNashef, Superoxide Ion: Generation and Chemical Implications, *Chem. Rev.*, 2016, **116**, 3029–3085.

70 S. O. Kim, C. V. Sastri, M. S. Seo, J. Kim and W. Nam, Dioxygen Activation and Catalytic Aerobic Oxidation by a Mononuclear Nonheme Iron(II) Complex, *J. Am. Chem. Soc.*, 2005, **127**, 4178–4179.

71 M. L. Pegis, J. A. S. Roberts, D. J. Wasylenko, E. A. Mader, A. M. Appel and J. M. Mayer, Standard Reduction Potentials for Oxygen and Carbon Dioxide Couples in Acetonitrile and N,N-Dimethylformamide, *Inorg. Chem.*, 2015, **54**, 11883–11888.

72 S. P. Schmidt, W. C. Trogler, F. Basolo, M. A. Urbancic and J. R. Shapley, Pentacarbonylrhenium Halides., *Inorg. Synth.*, 2007, **28**, 160–165.

73 D. A. Edwards and J. Marshalsea, The synthesis and spectral features of some cationic manganese(I) and rhenium(I) tricarbonyl complexes, *J. Organomet. Chem.*, 1977, **131**, 73–91.

74 J. A. Soderquist and C. L. Anderson, Crystalline anhydrous trimethylamine N-oxide, *Tetrahedron Lett.*, 1986, **27**, 3961–3962.

75 I. Noviandri, K. N. Brown, D. S. Fleming, P. T. Gulyas, P. A. Lay, A. F. Masters and L. Phillips, The Decamethylferrocenium/Decamethylferrocene Redox Couple: A Superior Redox Standard to the Ferrocenium/Ferrocene Redox Couple for Studying Solvent Effects on the Thermodynamics of Electron Transfer, *J. Phys. Chem. B*, 1999, **103**, 6713–6722.

76 D. Bao, B. Millare, W. Xia, B. G. Steyer, A. A. Gerasimenko, A. Ferreira, A. Contreras and V. I. Vullev, Electrochemical Oxidation of Ferrocene: A Strong Dependence on the Concentration of the Supporting Electrolyte for Nonpolar Solvents, *J. Phys. Chem. A*, 2009, **113**, 1259–1267.

77 *CrysAlisPro*, Version 1.171.36.28, Agilent Technologies, Santa Clara, CA, 2013.

78 (*a*) C. B. Hübschle, G. M. Sheldrick and B. Dittrich, ShelXle: A Qt Graphical User Interface for SHELXL, *J. Appl. Crystallogr.*, 2011, **44**, 1281–1284; (*b*) G. M. Sheldrick, SHELXT - Integrated Space-Group and Crystal-Structure Determination, *Acta Crystallogr., Sect. A: Found. Adv.*, 2015, **A71**, 3–8; (*c*) G. M. Sheldrick, Crystal Structure Refinement with SHELX, *Acta Crystallogr., Sect. C: Struct. Chem.*, 2015, **C71**, 3–8; (*d*) *International Tables for Crystallography*, Kluwer Academic Publishers, Dordrecht, Netherlands, 3rd edn, 2004, vol. C.

79 *SCALE3 ABSPACK-An Oxford Diffraction Program (1.0.4.Gui: 1.03)©*, 2005.

80 Bruker, *Apex-5 (Version 2023.9-4) and SAINT (Version 8.40B)*, Bruker AXS Inc., Madison, Wisconsin, USA, 2024.

81 (*a*) *SADABS (Version 2016/2)*, Bruker AXS Inc., Madison, Wisconsin, USA; (*b*) L. Krause, R. Herbst-Irmer, G. M. Sheldrick and D. Stalke, Comparison of Silver and Molybdenum Microfocus X-ray Sources for Single-Crystal Structure Determination, *J. Appl. Crystallogr.*, 2015, **48**, 3–10.

82 *XPREP (Version 2014/2)*, Bruker AXS Inc., Madison, Wisconsin, USA.

83 M. J. Frisch, G. W. Trucks, H. B. Schlegel, G. E. Scuseria, M. A. Robb, J. R. Cheeseman, G. Scalmani, V. Barone, G. A. Petersson, H. Nakatsuji, X. Li, M. Caricato, A. V. Marenich, J. Bloino, B. G. Janesko, R. Gomperts, B. Mennucci, H. P. Hratchian, J. V. Ortiz, A. F. Izmaylov, J. L. Sonnenberg, D. Williams-Young, F. Ding, F. Lipparini, F. Egidi, J. Goings, B. Peng, A. Petrone, T. Henderson, D. Ranasinghe, V. G. Zakrzewski, J. Gao, N. Rega, G. Zheng, W. Liang, M. Hada, M. Ehara, K. Toyota, R. Fukuda, J. Hasegawa, M. Ishida, T. Nakajima, Y. Honda, O. Kitao, H. Nakai, T. Vreven, K. Throssell, J. A. Montgomery Jr, J. E. Peralta, F. Ogliaro, M. J. Bearpark, J. J. Heyd, E. N. Brothers, K. N. Kudin, V. N. Staroverov, T. A. Keith, R. Kobayashi, J. Normand, K. Raghavachari, A. P. Rendell, J. C. Burant, S. S. Iyengar, J. Tomasi, M. Cossi, J. M. Millam, M. Klene, C. Adamo, R. Cammi, J. W. Ochterski, R. L. Martin, K. Morokuma, O. Farkas, J. B. Foresman and D. J. Fox, *Gaussiañ16 Revision C.01*, 2016.

84 Y. Zhao and D. G. Truhlar, The M06 suite of density functionals for main group thermochemistry, thermochemical kinetics, noncovalent interactions, excited states, and transition elements: two new functionals and systematic testing of four M06-class functionals and 12 other functionals, *Theor. Chem. Acc.*, 2008, **120**, 215–241.

85 N. Mardirossian and M. Head-Gordon, How Accurate Are the Minnesota Density Functionals for Noncovalent Interactions, Isomerization Energies, Thermochemistry, and Barrier Heights Involving Molecules Composed of Main-Group Elements?, *J. Chem. Theory Comput.*, 2016, **12**, 4303–4325.

86 F. Weigend, Accurate Coulomb-fitting basis sets for H to Rn, *Phys. Chem. Chem. Phys.*, 2006, **8**, 1057–1065.

87 F. Weigend and R. Ahlrichs, Balanced basis sets of split valence, triple zeta valence and quadruple zeta valence quality for H to Rn: Design and assessment of accuracy, *Phys. Chem. Chem. Phys.*, 2005, **7**, 3297–3305.

88 G. Scalmani and M. J. Frisch, Continuous surface charge polarizable continuum models of solvation. I. General formalism, *J. Chem. Phys.*, 2010, **132**, 114110.

89 G. Scalmani, M. J. Frisch, B. Mennucci, J. Tomasi, R. Cammi and V. Barone, Geometries and properties of excited states in the gas phase and in solution: Theory and application of a time-dependent density functional theory polarizable continuum model, *J. Chem. Phys.*, 2006, **124**, 094107.

90 M. E. Casida, C. Jamorski, K. C. Casida and D. R. Salahub, Molecular excitation energies to high-lying bound states from time-dependent density-functional response theory: Characterization and correction of the time-dependent local density approximation ionization threshold, *J. Chem. Phys.*, 1998, **108**, 4439–4449.

91 A. D. Laurent and D. Jacquemin, TD-DFT benchmarks: A review, *Int. J. Quantum Chem.*, 2013, **113**, 2019–2039.

92 L. E. Roy, E. Jakubikova, M. G. Guthrie and E. R. Batista, Calculation of One-Electron Redox Potentials Revisited. Is It Possible to Calculate Accurate Potentials with Density Functional Methods?, *J. Phys. Chem. A*, 2009, **113**, 6745–6750.

93 L. Rulíšek, On the Accuracy of Calculated Reduction Potentials of Selected Group 8 (Fe, Ru, and Os) Octahedral Complexes, *J. Phys. Chem. C*, 2013, **117**, 16871–16877.

94 J. H. Letcher and J. R. Van Wazer, Theoretical Interpretation of 31P NMR Chemical Shifts. I, *J. Chem. Phys.*, 1966, **44**, 815–829.

95 D. Purdela, Theory of ^{31}P NMR chemical shifts. II. Bond-angle dependence, *J. Magn. Reson.*, 1969, **1971**(5), 23–36.

96 J. Tong, S. Liu, S. Zhang and S. Z. Li, Prediction of 31P nuclear magnetic resonance chemical shifts for phosphines, *Spectrochim. Acta, Part A*, 2007, **67**, 837–846.

97 D. G. Gorenstein, *Phosphorous-31 NMR: Principles and Applications*, Academic Press Inc, New York, 1984.

98 J. B. Mann, T. L. Meek, E. T. Knight, J. F. Capitani and L. C. Allen, Configuration Energies of the d-Block Elements, *J. Am. Chem. Soc.*, 2000, **122**, 5132–5137.

99 L. C. Allen, Electronegativity is the average one-electron energy of the valence-shell electrons in ground-state free atoms, *J. Am. Chem. Soc.*, 1989, **111**, 9003–9014.